1996

Approximation of stability boundary of a power system using the real normal form of vector fields

Swapan Saha
Iowa State University

Approximation of stability boundary of a power system using the real normal form of vector fields

by

Swapan Saha

A Dissertation Submitted to the

Graduate Faculty in Partial Fulfillment of the

Requirements for the Degree of

DOCTOR OF PHILOSOPHY

Department: Electrical and Computer Engineering
Major: Electrical Engineering (Electric Power)

Approved:

Signature was redacted for privacy.

In Charge of Major Work

Signature was redacted for privacy.

For the Major Department

Signature was redacted for privacy.

For the Graduate College

Members of the Committee:

Signature was redacted for privacy.

Signature was redacted for privacy.

Signature was redacted for privacy.

Signature was redacted for privacy.

Iowa State University
Ames, Iowa
1996

TABLE OF CONTENTS

LIST OF TABLES

LIST OF FIGURES

NOMENCLATURE

δ_i	rotor angle of $i^{\underline{th}}$ machine
δ_{in}	rotor angle of $i^{\underline{th}}$ machine with respect to $n^{\underline{th}}$ machine
ω_i	rotor speed of $i^{\underline{th}}$ machine
ω_{in}	rotor speed of $i^{\underline{th}}$ machine with respect to $n^{\underline{th}}$ machine
M_i	inertia constant of $i^{\underline{th}}$ machine
D_i	damping constant of $i^{\underline{th}}$ machine
P_{mi}	mechanical power input to $i^{\underline{th}}$ machine
E_i	constant voltage behind the direct-axis transient reactance of $i^{\underline{th}}$ machine
G_{ii}	driving point conductance
Y_{ij}	modulus of $ij^{\underline{th}}$ element of the reduced system admittance matrix
θ_{ij}	argument of $ij^{\underline{th}}$ element of the reduced system admittance matrix
c	$= \frac{D_i}{M_i}, \quad \forall i$
A_{ij}	$= E_i E_j Y_{ij}$
n	number of generator
N	dimension of the system
$W^s(\hat{x})$	stable manifold of the equilibrium point $\hat{x}$
$W^u(\hat{x})$	unstable manifold of the equilibrium point $\hat{x}$

$A(x_S)$	region of attraction of stable equilibrium point x_S
$\partial A(x_S)$	stability boundary of stable equilibrium point x_S
U	matrix of right eigenvector
U_r	matrix of right real eigenvector
V_r^T	${U_r}^{-1}$
$h2_r$	real second order normal form coefficient
Γ_{ij}	curvature coefficient
λ	eigenvalue
$X_2(x), H$	2^{nd} order terms of the Taylor series (Hessian)
$Dh2_r(y)$	partial derivative of $h2_r(y)$ w. r. t. vector y
V_{PE}	potential energy
θ_i	machine angle of $i^{\underline{th}}$ machine in center of inertia (COI) reference
C_{ij}	$= E_i E_j B_{ij}$
D_{ij}	$= E_i E_j G_{ij}$
A	Jacobian matrix of the swing system
p_{ij}	participation factor of $i^{\underline{th}}$ state in the $j^{\underline{th}}$ mode

1. INTRODUCTION

1.1 Need for Analysis of Stressed Power Systems

Present interconnected power systems are much more stressed than ever due to lack of new transmission facility as well as heavier loading of the transmission network. This stress in a network exhibits several interesting but yet to understand nonlinear phenomena. This nonlinear complex behavior is not adequately analyzed with existing tools, and has generated considerable interest among researchers. Several nonlinear mathematical tools are being exploited with the existing procedures to investigate the nonlinear phenomenon in stressed power systems. This dissertation proposes the use of normal form of vector fields [1, 2], a comparatively new tool in the domain of power system analysis [3], to study the stability boundary of a stressed power system.

Earlier, several attempts were made by researchers to approximate the stability boundary of a power system. In a broad sense these approaches are of two categories: the first is Lyapunov/energy based, and the second is non Lyapunov type. A rigorous treatment of Lyapunov type methods is outside the scope of this dissertation and is available in the literature; see for example [4, 5]. We will only mention the salient features of some interesting works done in the area of characterization of stability boundary of a power system. Chiang et al [6] and Zaborzsky et al [7] independently

characterize the stability boundary of a power system. In these works the authors prove that under certain conditions the stability boundary of a power system is made of the union of stable manifold of the unstable equilibrium points (UEP) which lie on the boundary [8]. In other words, the boundary is known if the stable manifold of the UEP is known. It is extremely difficult, however, to numerically compute the stable manifold of an UEP for a practical size power network. To overcome this numerical computation problem, a constant energy surface through the UEP of interest is considered a good approximation of the stability boundary near that UEP.

In addition to the Lyapunov type method, a few other methods were tried to approximate the stability boundary of a power system. These methods were suggested nearly a decade ago; but none has been successfully applied to any practical size power system. The stability boundary has been approximated by a power series and the coefficients are calculated by considering the properties of the stability boundary at a "type-1" UEP [9]. Type-1 UEP is defined in chapter 2. The stability boundary of a SEP is assumed to be made of a number of disjoint $(2n-3)$ surfaces in a $(2n-2)$ space [10], n being number of generators. $(2n-3)$ planes, tangent to the stability boundary at the type-1 UEP, are constructed to approximate the stability boundary. In other words, the union of eigenvectors at the type-1 UEP is taken as the approximate stability boundary. This approximation is, however, a first order approximation. A power series expansion of the stable manifold of a "hyperbolic" equilibrium point is derived in [11], which was inspired by Ushiki's work [12]. Ushiki introduced explicit globally analytic expressions of unstable manifolds for strictly hyperbolic equilibrium points. The idea of the hyperplane has been extended to find the second order approximation to the stability boundary [13]. Recently, artificial neural network

based tangent hypersurfaces have been proposed in [14] to approximate the stability boundary.

In this dissertation, we suggest a methodology to approximate the stable manifold of an UEP using the normal form theory. The key idea of this method is that for a linear system the stable manifold is equivalent to the stable eigenspace. The nonlinear system is transformed to a linear system by a nonlinear coordinate transformation. The stable eigenspace of the transformed linear system is transformed back to the original coordinates using the nonlinear transformation resulting in an approximated stable manifold. The objective of this research is to develop new methods or combinations of methods to analyze, and explain the nonlinear phenomena in stressed power systems.

1.2 Method of Normal Forms

Normal form theory gives a tool for simplifying the forms of equations to the simplest possible higher-order terms near their equilibria [1, 2, 15, 16, 17]. The key idea underlying the normal form method is the use of *local* coordinate transformations to *simplify* the equations describing the system dynamics under considerations. In other words, with the normal form method a dynamical system is transformed to the *simplest form* or so-called *normal form* system using nonlinear coordinate transformation. The next chapter describes the normal form method in detail.

The key idea of this dissertation is to approximate the stable manifold of an unstable equilibrium point using the normal form method. The original nonlinear system is transformed to a linear system using the nonlinear coordinate transform around an equilibrium point. Then the stable eigenspace of the *transformed linear*

system is transformed back to the original system to approximate the stable manifold of the original nonlinear system up to some degree. This approximate stable manifold is used to find the stability boundary of a stable equilibrium point around the unstable equilibrium point of interest. Thus, the normal form method enables us to approximate the stable manifold of this unstable equilibrium point which is otherwise very difficult to compute numerically for a practical size power system.

This method involves two steps: 1) first to select an unstable equilibrium point (UEP) which lies on the stability boundary, and 2) the second step is to approximate the boundary by the second order approximated manifolds. Direct stability analysis involves calculation of a value of critical potential energy against which transient stability assessment is made. There are several UEPs on the stability boundary. The UEP of interest is called the controlling UEP and its computation is one of the key steps in power system transient stability assessment by the transient energy function (TEF) method [5]. Thus, we can assume that computation of (at least some of) the UEPs on the stability boundary is feasible.

The method of normal forms of vector fields is being used to characterize the dynamic behavior of stressed power systems at Iowa State University [18]. In [19], this method is applied to characterize the mode-state participation and understand the relationship between system stressed condition and nonlinearity. The nonlinear modal interaction and the effect of the interaction on the stressed power system dynamic behavior including excitation control performance are discussed in [20]. The normal form method is also applied to the analysis of the ac/dc power system dynamics [21]. Additional work, using normal forms method, to predict the inter-area type system separation in a large power system is also undertaken. In all of this work, the

analysis is done around the stable equilibrium point. However, as mentioned above, this dissertation also contains analysis of a stressed power system around the relevant unstable equilibrium point.

1.3 Problem Statement

The objective of the present work is to understand "better" the nonlinear phenomenon of stressed power systems. The prediction of the location of boundaries between groups of machines, during system separation following a large disturbance is of great interest. A novel method of approximation of the stability boundary of a stable equilibrium point around an unstable equilibrium point will be presented. The emphasis is to study the effect of system stress on the stability boundary of a power system. Analysis of how the shape of the boundary is affected by stress is of interest. The stability boundary will be approximated using the normal form of vector fields. The approximated boundary will then be examined to see whether it gives a proper estimation of critical energy. The behavior of the system trajectory near the UEP will be investigated to find how the unstable trajectory leaves the boundary.

1.4 Organization of the Dissertation

The organization of this dissertation is as follows; the introduction presents a motivation, and general overview of the proposed method. Chapter 2, which provides a review of the related dynamical system, presents the formulation of the problem including the modeling of the system and also contains the motivation for real normal form of vector fields. In chapter 3, the general method of approximation of the stability boundary is presented. First, linear analysis around the unstable equilibrium

point is provided, then it is followed by the method of approximation of the stable manifold by the real normal form of vector fields. Display of the boundary, computation of potential energy, and solution steps are given at the end of the chapter 3. The numerical examples of the proposed method on an 11 generator test system, as well as the effect of stress on the shape, size of the region of attraction and stability boundary, and movement of the equilibrium points are described in chapter 4. Chapter 5 describes a conceptual framework to study the mode of system instability as an application of the approximate boundary. Conclusions and suggestions for future work are presented in chapter 6. Finally the Acknowledgments, Bibliography are followed by the appendices described in the following paragraph.

The derivation of Jacobian and Hessian matrices are given in Appendix A. Appendix B contains the machine data and load flow data for the 11 generator test system.

2. MATHEMATICAL FORMULATION

Before presenting the proposed methodology, we will briefly review a few terminology commonly used in characterization of stability boundary of the power systems [22, 23].

2.1 Review of Related Dynamic Systems

A power system can be described as a nonlinear autonomous system and is denoted as

$$\dot{x} = f(x) \tag{2.1}$$

where the vector field f maps R^N into R^N and is continuously differentiable. A point, $\hat{x}$ is called as an *equilibrium point* (EP) or a *fixed point* of equation (2.1) if $f(\hat{x}) = 0$. The derivative of the function f at $\hat{x}$ is known as the Jacobian matrix. When the Jacobian matrix at an equilibrium point has no eigenvalues with a zero real part, the equilibrium point is called *hyperbolic.* If the Jacobian of the equilibrium point, $\hat{x}$ has m eigenvalues with positive real part, it is called a *type-m UEP.* The solution curve of equation (2.1) starting initial state x at $t = 0$ is called a *trajectory,* and denoted by $\phi(x, .)$. The *stable* and *unstable manifold,* $W^s(\hat{x})$ and $W^u(\hat{x})$ of the hyperbolic equilibrium point, $\hat{x}$ are defined as

$$W^s(\hat{x}) = \{x : \phi(x,t) \overset{\exp}{\rightarrow} \hat{x} \ \ as \ \ t \rightarrow \infty\} \tag{2.2}$$

$$W^u(\hat{x}) = \{x : \phi(x,t) \overset{\exp}{\rightarrow} \hat{x} \ \ as \ \ t \rightarrow -\infty\} \tag{2.3}$$

The physical meaning of the stable manifold of an equilibrium point is that if a trajectory touches a stable manifold, the trajectory converges to the equilibrium point, whenever the trajectory hits the unstable manifold it goes away from the equilibrium point when time increases.

For a stable equilibrium point (SEP), there is a region in the state space from which all trajectories converge to x_S as $t \rightarrow \infty$ and this region is known as *region of stability* of x_S and is denoted by $A(x_S)$. The stability boundary is the boundary of the region of stability, is denoted by $\partial A(x_S)$.

For a linear system, stable eigenspace is equivalent to stable manifold. But for a nonlinear system stable eigenspace is a linear approximation to stable manifold and the former is tangent to the latter at the equilibrium point. This can be explained with Figure 2.1. With this introduction, we now formulate the problem to be studied in this work.

2.2 Machine and Load Model

We consider the classical model of multimachine system. Loads are treated as constant impedances and the system is reduced to the internal machine buses. The equation of motion can be written as the state-space equations [24].

$$\dot{\delta}_i = \omega_i \quad for \ \ i = 1, ..., n$$

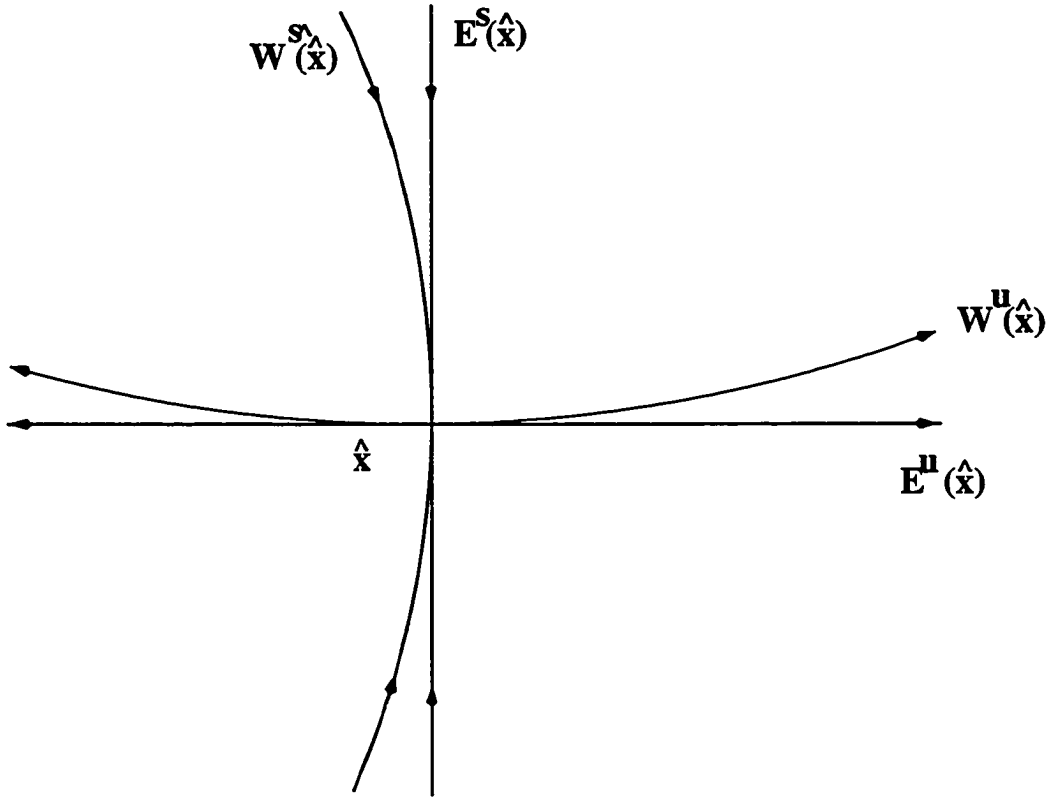

Figure 2.1: Eigenspace and local invariant manifold of a nonlinear system at an equilibrium point, $\hat{x}$

$$\dot{\omega}_i = f_i(\delta,\omega) = \frac{1}{M_i}\left[P_{mi} - D_i\omega_i - E_i^2 G_{ii} - \sum_{j=1,i\neq j}^{n} E_i E_j Y_{ij}\cos(\delta_i - \delta_j - \theta_{ij})\right] \tag{2.4}$$

As the synchronism depends on the rotor-angle differences and not on their magnitude, relative angles, and speeds are used as system state variables. Accordingly, the $n^{\underline{th}}$ machine is taken as reference. Now defining,

$\delta_{in} = \delta_i - \delta_n$ and $\omega_{in} = \omega_i - \omega_n$ the equation (2.4) can be rewritten as

$$\begin{aligned}
\dot{\delta}_{in} &= \omega_{in} \quad for \;\; i = 1,..,n-1 \\
\dot{\omega}_{in} &= \frac{1}{M_i}\left(P_{mi} - E_i^2 G_{ii}\right) - \frac{1}{M_n}\left(P_{mn} - E_n^2 Gnn\right) \\
&\quad -\frac{1}{M_i}\left[E_i E_n Y_{in}\cos\left(\delta_{in} - \theta_{in}\right) + \sum_{j=1,j\neq i}^{n-1} E_i E_j Y_{ij}\cos\left(\delta_{in} - \delta_{jn} - \theta_{ij}\right)\right] \\
&\quad +\frac{1}{M_n}\left[\sum_{j}^{n-1} E_j E_n Y_{jn}\cos\left(\delta_{jn} + \theta_{jn}\right)\right] - c\,\omega_{in} \qquad i = 1,...,n-1
\end{aligned} \tag{2.5}$$

where, δ_i is the rotor angle of $i^{\underline{th}}$ machine

δ_{in} is the rotor angle of $i^{\underline{th}}$ machine with respect to $n^{\underline{th}}$ machine

ω_i is the rotor speed of $i^{\underline{th}}$ machine

ω_{in} is the rotor speed of $i^{\underline{th}}$ machine with respect to $n^{\underline{th}}$ machine

M_i is the inertia constant of $i^{\underline{th}}$ machine

D_i is the damping constant of $i^{\underline{th}}$ machine

P_{mi} is the mechanical power input to $i^{\underline{th}}$ machine

E_i is the constant voltage behind the direct-axis transient reactance of $i^{\underline{th}}$ machine

G_{ii} is the driving point conductance

Y_{ij} is the modulus of $ij^{\underline{th}}$ element of the reduced system admittance matrix

θ_{ij} is the argument of $ij^{\underline{th}}$ element of the reduced system admittance matrix $c = \frac{D_i}{M_i}$ is constant for uniform damping. The value of c is taken as 0.1 in this work. Equation (2.5) represents the swing system. For n generator system, the number of state variables are $2(n-1)$. In general, equation (2.5) can be represented by equation (2.1).

Now we present the formulation for the real normal form transformation [25].

2.3 Real Normal Form of Vector Fields

Expanding equation (2.1) around an equilibrium point we get,

$$\dot{x} = Ax + X_2(x) + H.O.T \qquad x \in R^N \tag{2.6}$$

and for the $i^{\underline{th}}$ variable, x_i

$$\dot{x_i} = A_i x + \frac{1}{2} x^T H^i x + H.O.T \tag{2.7}$$

where,

$A_i = i^{\underline{th}}$ row of Jacobian matrix A which is given by $\left[\frac{\partial f}{\partial x}\right]_{x_o}$, x_o is an equilibrium point, and $H^i = \left[\frac{\partial^2 f_i}{\partial x_i \partial x_j}\right]_{x_o}$ = Hessian matrix. The detail for the derivation of the Jacobian matrix A and the Hessian matrices H^i of the system is given in Appendix A.

In this formulation, terms higher than second order in equation (2.6) are neglected. We do the similarity transformation using equation (2.8)

$$x = U_r y \qquad y \in R^N \tag{2.8}$$

U_r is formed from complex right eigenvectors of A, U. From a complex conjugate pair of eigenvectors corresponding to a complex conjugate pair of eigenvalues of A,

the real and imaginary components are taken separately to form two columns of U_r matrix. Equation (2.6), after similarity transformation becomes

$$\dot{y} = J_r y + Y_2(y) \qquad y \in R^N \tag{2.9}$$

and for the $j^{\underline{th}}$ mode, assuming it to be a real mode

$$\begin{aligned} \dot{y_j} &= \lambda_j y_j + y^T C^j y \\ &= \lambda_j y_j + \sum_{k=1}^{N} \sum_{l=k}^{N} C^j_{kl} y_k y_l \end{aligned} \tag{2.10}$$

where $C^j = \frac{1}{2} \sum_{p=1}^{N} V_r^T{}_{jp} [U_r^T H^p U_r] = [C^j_{kl}]$, and $V_r^T = U_r{}^{-1}$

We now introduce nonlinear coordinate transformation

$$y = z + h2_r(z) \qquad z \in R^N \tag{2.11}$$

If "resonance" conditions are satisfied (see discussion of equation (2.15) below), we get the transformed linear system as

$$\dot{z} = J_r z \tag{2.12}$$

The $h2_r s$ are obtained solving the following homological equation,

$$La\, h2_r = Y_2 \tag{2.13}$$

La is known as *Lie (or Poisson) bracket* [1] of vector fields $J_r y$ and $h2_r(y)$, and is given by

$$Lah2_r(y) = \{Dh2_r(y) J_r y - J_r h2_r(y)\} \tag{2.14}$$

where $Dh2_r(y)$ is the Jacobian matrix of the vector $h2_r(y)$.

If we do complex normal form transformation, we can simplify the computation of $h2$ coefficients [1] as follows:

$$h2^i_{jk} = \frac{C^i_{jk}}{\lambda_j + \lambda_k - \lambda_i} \tag{2.15}$$

In the complex normal form approach, a set of N-dimensional system modes is said to be resonant of order r (where r is an integer), if $\lambda_i = \sum_{j=1}^{N} m_j \lambda_j$ and $r = \sum_j^N m_j$ for $i = 1, .., N$; λ being a vector of eigenvalues. The linear operator La is diagonal. In other words, under resonant condition the linear operator La is not invertible. It is characterized by $\lambda_j + \lambda_k = \lambda_i$ for second-order resonance condition. In the real normal form transformation, the notion of resonance is the same as far as the invertibility of the linear operator La of equation (2.14) is concerned. But the only difference is in the derivation of the condition of resonance as La is not diagonal (see Section 2.5).

The resonant nonlinear terms of a normal form are those ones that cannot be eliminated by a nonlinear polynomial change of variable [26]. Technically they are in the kernel of the adjoint of the homological operator, La.

Linear stable eigenspaces of the "transfomed linear system" of the z system given by the equation (2.12), are transformed back to x system to approximate the stable manifolds.

2.4 Motivation of Real Normal Forms

In our work we transform the state variables back and forth from x to z space via y space. Figure 2.2 corresponds to the case when the conventional complex similarity

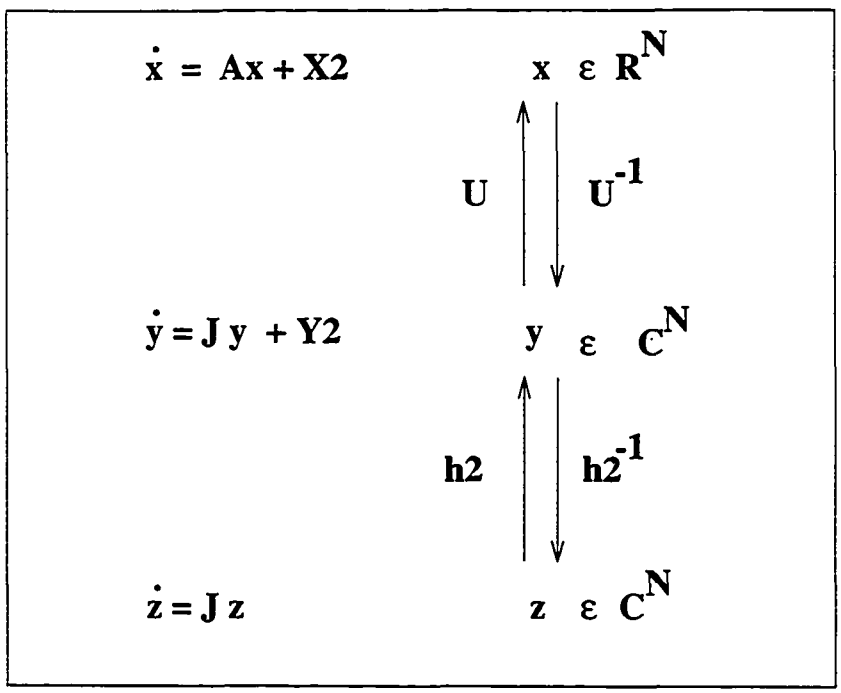

Figure 2.2: Complex normal form transformation

and normal form transformation are performed. We get a point in complex space when any point in the z space is transformed back to the x space. The problem arises, when we attempt to connect all the points in x space to approximate the manifold, and hence the boundary. We alleviate this problem using real form transformation. Figure 2.3 shows the case for all real transformations.

Let us assume that we approximate the stability boundary around a type-1 UEP. This UEP has $N-1$ dimensional stable manifold and 1 dimensional unstable manifold. The stability boundary around this UEP is made of this $N-1$ dimensional stable manifold. This $N-1$ stable manifold will be approximated by using corresponding stable eigenspace, and normal form transformation.

In this dissertation the region of the stability is approximated by the real normal form method near the so-called controlling UEP. This is the UEP, the potential energy of which represents the critical energy for the particular disturbance under investigation (see chapter 5 of [5]).

2.5 An Example of La for 2 Dimensional System

Let us assume for a two dimensional system we have the Jordan system as given by

$$J_r = \begin{bmatrix} \mu & \nu \\ -\nu & \mu \end{bmatrix} \tag{2.16}$$

Let $y = [y_1, y_2]^T$. Eigenvalues of J_r are $(\mu \pm j\nu)$. Let us use second order terms as

$$H_2 = span\left\{ \begin{pmatrix} y_1^2 \\ 0 \end{pmatrix}, \begin{pmatrix} y_1 y_2 \\ 0 \end{pmatrix}, \begin{pmatrix} y_2^2 \\ 0 \end{pmatrix}, \begin{pmatrix} 0 \\ y_1^2 \end{pmatrix}, \begin{pmatrix} 0 \\ y_1 y_2 \end{pmatrix}, \begin{pmatrix} 0 \\ y_2^2 \end{pmatrix} \right\}$$

Now we compute $La(.)$ using the equation (2.14) as follows [17].

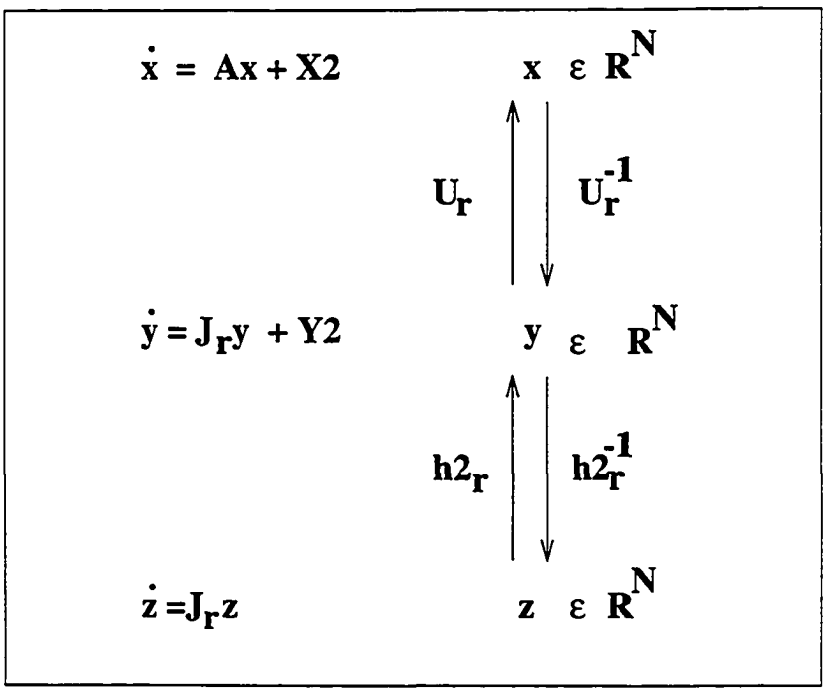

Figure 2.3: Real normal form transformation

$$La\begin{pmatrix} y_1^2 \\ 0 \end{pmatrix} = \begin{pmatrix} 2y_1 & 0 \\ 0 & 0 \end{pmatrix}\begin{pmatrix} \mu y_1 + \nu y_2 \\ -\nu y_1 + \mu y_2 \end{pmatrix} - \begin{pmatrix} \mu & \nu \\ -\nu & \mu \end{pmatrix}\begin{pmatrix} y_1^2 \\ 0 \end{pmatrix}$$

$$= \begin{pmatrix} \mu y_1^2 + 2\nu y_1 y_2 \\ \nu y_1^2 \end{pmatrix}$$

$$La\begin{pmatrix} y_1 y_2 \\ 0 \end{pmatrix} = \begin{pmatrix} y_2 & y_1 \\ 0 & 0 \end{pmatrix}\begin{pmatrix} \mu y_1 + \nu y_2 \\ -\nu y_1 + \mu y_2 \end{pmatrix} - \begin{pmatrix} \mu & \nu \\ -\nu & \mu \end{pmatrix}\begin{pmatrix} y_1 y_2 \\ 0 \end{pmatrix}$$

$$= \begin{pmatrix} \mu y_1 y_2 + \nu y_2^2 - \nu y_1^2 \\ \nu y_1 y_2 \end{pmatrix}$$

$$La\begin{pmatrix} y_2^2 \\ 0 \end{pmatrix} = \begin{pmatrix} 0 & 2y_2 \\ 0 & 0 \end{pmatrix}\begin{pmatrix} \mu y_1 + \nu y_2 \\ -\nu y_1 + \mu y_2 \end{pmatrix} - \begin{pmatrix} \mu & \nu \\ -\nu & \mu \end{pmatrix}\begin{pmatrix} y_2^2 \\ 0 \end{pmatrix}$$

$$= \begin{pmatrix} \mu y_2^2 - 2\nu y_1 y_2 \\ \nu y_2^2 \end{pmatrix}$$

$$La\begin{pmatrix} 0 \\ y_1^2 \end{pmatrix} = \begin{pmatrix} 0 & 0 \\ 2y_1 & 0 \end{pmatrix}\begin{pmatrix} \mu y_1 + \nu y_2 \\ -\nu y_1 + \mu y_2 \end{pmatrix} - \begin{pmatrix} \mu & \nu \\ -\nu & \mu \end{pmatrix}\begin{pmatrix} 0 \\ y_1^2 \end{pmatrix}$$

$$= \begin{pmatrix} -\nu y_1^2 \\ 2\nu y_1 y_2 + \mu y_1^2 \end{pmatrix}$$

$$La\begin{pmatrix} 0 \\ y_1 y_2 \end{pmatrix} = \begin{pmatrix} 0 & 0 \\ y_2 & y_1 \end{pmatrix}\begin{pmatrix} \mu y_1 + \nu y_2 \\ -\nu y_1 + \mu y_2 \end{pmatrix} - \begin{pmatrix} \mu & \nu \\ -\nu & \mu \end{pmatrix}\begin{pmatrix} 0 \\ y_1 y_2 \end{pmatrix}$$

$$= \begin{pmatrix} -\nu y_1 y_2 \\ \mu y_1 y_2 - \nu y_1^2 + \nu y_2^2 \end{pmatrix}$$

$$La \begin{pmatrix} 0 \\ y_2^2 \end{pmatrix} = \begin{pmatrix} 0 & 0 \\ 0 & 2y_2 \end{pmatrix} \begin{pmatrix} \mu y_1 + \nu y_2 \\ -\nu y_1 + \mu y_2 \end{pmatrix} - \begin{pmatrix} \mu & \nu \\ -\nu & \mu \end{pmatrix} \begin{pmatrix} 0 \\ y_2^2 \end{pmatrix}$$

$$= \begin{pmatrix} -\nu y_2^2 \\ -2\nu y_1 y_2 + \mu y_2^2 \end{pmatrix}$$

Now we represent a matrix representation of the linear operator $La(.)$ with the above expressions

$$La(.) = \begin{pmatrix} \mu & -\nu & 0 & -\nu & 0 & 0 \\ 2\nu & \mu & -2\nu & 0 & -\nu & 0 \\ 0 & \nu & \mu & 0 & 0 & -\nu \\ \nu & 0 & 0 & \mu & -\nu & 0 \\ 0 & \nu & 0 & 2\nu & \mu & -2\nu \\ 0 & 0 & \nu & 0 & \nu & \mu \end{pmatrix} \tag{2.17}$$

An example of normal form based computation of unstable manifold of an equilibrium point is discussed below.

2.6 Unstable Manifold by Normal Form Method - An Example

Let us consider the following vector field (page 23 [17]).

$$\begin{aligned} \dot{x_1} &= x_1 \\ \dot{x_2} &= -x_2 + x_1^2, \quad (x_1, x_2) \in R \times R \end{aligned} \tag{2.18}$$

The linear part of (2.18) is given as

$$A = \begin{bmatrix} 1 & 0 \\ 0 & -1 \end{bmatrix}$$

which has a hyperbolic equilibrium point at $(x_1, x_2) = (0, 0)$. The unstable manifold of the equilibrium point, $(0, 0)$ is given in [17] as

$$W^u(0,0) = \left\{(x_1, x_2) \in R^2 \mid x_2 = \frac{1}{3}x_1^2\right\}. \tag{2.19}$$

Equation (2.19) is graphically shown in Figure 2.4.

Next the unstable manifold of the EP is computed using the normal form method. Eigenvalues of (2.18) are $1, -1$. The matrix of right eigenvectors, U is given as

$$U = \begin{bmatrix} 1 & 0 \\ 0 & 1 \end{bmatrix}$$

Since the system is already in Jordan form ($here, J = A$), following the notation used in section 2.3, the system can be written as

$$\begin{aligned} \dot{y_1} &= y_1 \\ \dot{y_2} &= -y_2 + y_1^2 \end{aligned} \tag{2.20}$$

Nonlinear coefficients are computed as:

$$h2_{11}^1 = h2_{12}^1 = h2_{22}^1 = h2_{12}^2 = h2_{22}^2 = 0$$

$$h2_{11}^2 = \frac{C_{11}^2}{\lambda_1 + \lambda_1 - \lambda_2} = \frac{1}{3}$$

Hence, the nonlinear transformation is given by

$$\begin{aligned} y_1 &= z_1 \\ y_2 &= z_2 + \frac{1}{3}z_1^2 \end{aligned} \tag{2.21}$$

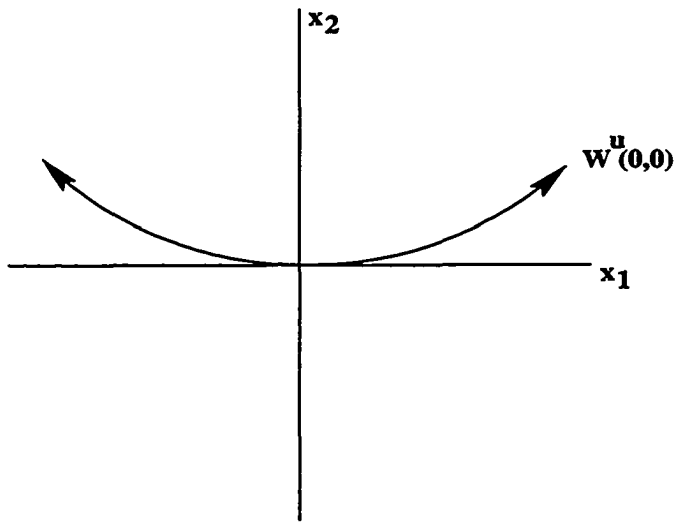

Figure 2.4: Unstable manifold at EP, (0,0)

Now unstable eigenspace in the z-space corresponding to eigenvalue 1 is given by:

$$E^u(0,0) = \left\{(z_1, z_2) \in R^2 \mid z_2 = 0\right\}$$

Transforming the above relation to the y-space and then to the x-space

$$\begin{aligned} x_1 &= z_1 \\ x_2 &= \frac{1}{3}z_1^2 \end{aligned} \tag{2.22}$$

which simplifies to $x_2 = \frac{1}{3}x_1^2$. This can be written as in (2.19). Hence, using the normal form transformation and associated unstable eigenspace, the unstable manifold of an equilibrium point is computed.

2.7 Summary

This chapter provides the background materials for the normal form method to approximate the stability boundary around the UEP of interest. The motivation for

real normal form method has been discussed. The key idea of normal form method has been explained. For normal form method several interesting articles are available in the literature. Authors in [27, 28] provide the basic concept, foundation on the modern theory of normal forms for nonlinear vector fields. An example of La operator for real normal form transformation is also presented in this chapter. The concept of normal form based approximation of invariant manifold is explained with a simple example in this chapter. The next chapter will present a systematic procedure to approximate the stability boundary around the UEP of interest.

3. APPROXIMATION OF STABILITY BOUNDARY

3.1 Linear Analysis around the UEP

Equation (2.1) is expanded at an UEP by Taylor series. The Jacobian of the Taylor series is used to find the eigenvalues, and eigenvectors. The linear system of (2.1) is given by

$$\dot{x} = Ax \tag{3.1}$$

Matrix A is $N \times N$. If A has N distinct eigenvalues then it will also have N corresponding linearly independent $N \times 1$ right eigenvectors U_i, $i = 1, N$ and $N \times 1$ left eigenvectors V_i, which are related by the following equations:

$$AU_i = \lambda_i U_i \qquad i = 1, ..., N \tag{3.2}$$

$$A^T V_j = \lambda_j V_j \qquad j = 1, ..., N \tag{3.3}$$

Let U be a matrix of right eigenvectors U_i and V be a matrix of left eignevectors, then we have the following relationship:

$$V^T U = I_N \tag{3.4}$$

where I_N is $N \times N$ identity matrix. The so-called participation factor [29], p_{ij}, is given by,

$$p_{ij} = V_{ij} U_{ij} \tag{3.5}$$

Physically the participation factor p_{ij} gives a measure of the participation of $i^{\underline{th}}$ state variable in the $j^{\underline{th}}$ mode.

3.2 Coefficient of Curvature

Let us consider $\hat{z} = \{0, .., \hat{z_j}, ..., 0\}$ be any point in the z-space, where $\hat{z_j}$ is any constant number, say 1.0. This point can be transformed to y-space via $y = z + h2_r(z)$ as $\hat{y} = \{\hat{y_1}, ..., \hat{y_N}\}$, where

$$\hat{y_i} = \hat{z_i} + \sum_{j=1}^{N} \sum_{k=j}^{N} h\dot{2}^{i}_{rjk} \hat{z_j} \hat{z_k}, \quad i = 1, N \tag{3.6}$$

Further substitution of $\hat{z}$ gives:

$$\hat{y_i} = h\dot{2}^{i}_{rjj} \hat{z_j}^2, i \neq j, \quad i = 1, N$$

$$\hat{y_j} = \hat{z_j} + h\dot{2}^{j}_{rjj} \hat{z_j}^2 \tag{3.7}$$

When we transform back $\hat{y}$ to the x-space via $x = U_r y$ we get $\hat{x}$ which can be written as $\hat{x} = \{\hat{x_1}, ..., \hat{x_N}\}$.

In compact form we can write

$$\hat{x_i} = U_{rij} \hat{z_j} + (U_{ri1} h2^{1}_{rjj} + ... + U_{riN} h2^{N}_{r\ jj}) \hat{z_j}^2 \tag{3.8}$$

$$= U_{rij} \hat{z_j} + \Gamma_{ij} \hat{z_j}^2, \ i = 1, ..., N$$

where $\Gamma_{ij} = [U_{ri1} h2^{1}_{rjj} + ... + U_{riN} h2^{N}_{r\ jj}]$. From equation (3.8), we get

$$\frac{\partial^2 \hat{x_i}}{\partial \hat{z_j}^2} = 2\Gamma_{ij} \tag{3.9}$$

From the above expressions, we can correlate any particular state variable $\hat{x_i}$ to the curvature which is given by $h2_r$. The main point is that instead of using only $h2_r$,

we can use the sum of the product given by Γ_{ij} to find how the curvature is reflected in the i^{th} state variable, $\hat{x_i}$ due to the j^{th} mode. The product as mentioned will be used as a measure to indicate the curvature along a system variable direction.

Hence, a new parameter Γ is used to define a relationship between the state variable i and the curvature due to mode j:

$$\Gamma_{ij} = \sum_{k=1}^{N} U_{rik} h2^{k}_{rjj} \tag{3.10}$$

The way the above formulation is made is to find a relation between a state variable i and a mode j. It is also possible to find a new parameter Γ^{i}_{jk} to find a relation among a state i and two modes j and k. The idea for this derivation is as follows. In the previous formulation, only one component in a particular direction in the z-space is considered. As an example, for a vector {0,0,....,α,...,0} in the z-space, Γ_{ij} is computed. Now considering all nonzero elements in any particular direction, we have

$$x_i = \sum_{j=1}^{N} U_{rij} y_j \tag{3.11}$$

Where y_j is given by

$$y_j = z_j + \sum_{k=1}^{N} \sum_{l=k}^{N} h2^{j}_{rkl} z_k z_l \tag{3.12}$$

Hence, we get x_i as

$$x_i = \sum_{j=1}^{N} U_{rij} z_j + \sum_{j=1}^{N} U_{rij} \sum_{k=1}^{N} \sum_{l=k}^{N} h2^{j}_{rkl} z_k z_l \tag{3.13}$$

From equation (3.13) the following parameter is derived to find a relation among a state i and two modes j and k as follows.

$$\Gamma^{i}_{jk} = \frac{\partial^2 x_i}{\partial z_j \partial z_k} \tag{3.14}$$

The above expression can be written explicitly in terms of $h2_r$ and U_r. From equation (3.13) the following relation among a state i and two modes j and k is obtained:

$$\frac{\partial^2 x_i}{\partial z_j \partial z_k} = 2 \sum_{l=1}^{N} U_{ril} h2^l_{rjk} \tag{3.15}$$

Hence,

$$\Gamma^i_{jk} = \sum_{l=1}^{N} U_{ril} h2^l_{rjk} \tag{3.16}$$

3.3 Approximation of the Manifold of the UEP

As the system represented by equation (2.12) is linear and diagonal, the eigenvector corresponding to the system is obtained as a canonical set of vectors.

For the normal form system, we get $N-1$ dimensional stable manifold, and 1 dimensional unstable manifold associated with the type-1 UEP. This $N-1$ stable manifold is represented by $N-1$ straight lines in the z-space. They are given as $[\alpha_1, 0, ..., , ..0]^T$, $[0, \alpha_2, 0, ..., 0]^T$, $...[0, ...\alpha_i, 0, .., 0]^T$, α_i is a real number; where $i = 1, ..N$ and $i \neq j$; $j^{\underline{th}}$ mode is unstable. Now if we transform the $i^{\underline{th}}$ stable eigenvector to the y coordinate, we get $[h2^1_{ii}\alpha_i^2, ..., \alpha_i + h2^i_{ii}\alpha_i^2, 0, ..., h2^N_{ii}\alpha_i^2]^T$. This $i^{\underline{th}}$ stable eigenvector in zi coordinate space can be further transformed back to the x coordinate space as $[U_{1i}h2^1_{ii}\alpha_i^2, ..., U_{ii}(\alpha_i + h2^i_{ii}\alpha_i^2)., U_{Ni}h2^N_{ii}\alpha_i^2]^T$.

As done for the $i^{\underline{th}}$ stable eigenvector, we can transform all the $N-1$ stable eigenvectors to the original x coordinate. Thus, we approximate the stable manifold up to the higher order term retained in the Taylor series expression (second order in this dissertation).

3.4 Display of Boundary

Under certain conditions (see [6]) the stability boundary of an SEP is the union of the stable manifolds of the UEPs on the boundary. Near each UEP an approximation of the stability boundary can be obtained as follows: compute the normal form at the UEP (in this work up to 2^{nd} order); approximate the stable manifold in the z-space by the stable subspace; transform this subspace using U_r and $h2_r$ back into the x-space, i.e., to the machine variables. For a type-1 UEP stability boundary around the UEP is an $(N-1)$ dimensional hypersurface in N dimensional space. For a large power system, it is not possible to display the boundary in the large dimensional space. Hence, select a 3 dimensional angular subspace to display the approximated stability boundary graphically. In most angular directions, the stable manifold is relatively 'flat' i.e. looks like a subspace. The important directions are those with high Γ coefficients, usually they are the variables corresponding to the advanced machines in the UEP.

3.5 Potential Energy

The system of equations is formulated in synchronous reference frame with the n^{th} machine taken as reference. With uniform damping we have $2n-2$ state variables for an n machine system. They are $\{\delta_{1n}, \delta_{2n}, ..., \delta_{n-1,n}, \omega_{1n}, .., \omega_{n-1,n}\}$.

The closed form expression of energy in the center of inertia (COI) reference frame [5] is used here. Using the linear angle path assumption for the dissipation terms between a point on the boundary, θ^b, and the postfault SEP, θ^s the potential energy is given by:

$$V_{PE} = -\sum_{i=1}^{n} P_i \left(\theta_i^b - \theta_i^s\right) - \sum_{i=1}^{n-1} \sum_{j=i+1}^{n} [C_{ij}(cos\theta_{ij}^b - cos\theta_{ij}^s) - D_{ij} I_{ij}(sin\theta_{ij}^b - sin\theta_{ij}^s)] \quad (3.17)$$

Where $I_{ij} = \frac{\theta_i^b - \theta_i^s + \theta_j^b - \theta_j^s}{\theta_{ij}^b - \theta_{ij}^s}$ and $P_i = P_{mi} - E_i^2 G_{ii}$. To use the energy expression in COI frame, the following relationship is made [30]:

$$\begin{bmatrix} \delta_{1n} \\ \delta_{2n} \\ \cdots \\ \delta_{n-1,n} \end{bmatrix} = \begin{bmatrix} 1+\frac{M_1}{M_n} & \frac{M_2}{M_n} & ..... & \frac{M_{n-1}}{M_n} \\ \frac{M_1}{M_n} & 1+\frac{M_2}{M_n} & ..... & \frac{M_{n-1}}{M_n} \\ \frac{M_1}{M_n} & \frac{M_2}{M_n} & ..... & \frac{M_{n-1}}{M_n} \\ \frac{M_1}{M_n} & \frac{M_2}{M_n} & ..... & 1+\frac{M_{n-1}}{M_n} \end{bmatrix} \begin{bmatrix} \theta_1 \\ \theta_2 \\ \cdots \\ \theta_{n-1} \end{bmatrix} \quad (3.18)$$

$$\theta_n = -\frac{1}{M_n} \sum_{i=1}^{n-1} M_i \theta_i \quad (3.19)$$

In the above expression, θ is in the COI frame. The approach used is as follows. We will pick up several points in the z-space on the linear manifold. These points (in the z-space) are transformed to the x-space (see section 3.3). The points obtained in the x-space are real. These points will be substituted in the energy expression to find the energy.

3.6 Computation of Distance

In this dissertation, the distance between a postfault SEP θ^s and any point θ on any manifold as is given by:

$$\sqrt{\sum_{i=1}^{N} (\theta(i) - \theta^s(i))^2}$$

where N is dimension of the system. The norm defined, as above is known as norm-2.

3.7 Computational Steps

For any operating condition the following steps are performed to find an approximate estimate of the stability boundary for a power system, near the controlling UEP.

1. Reduce the power system network to the internal machine buses.
2. Find the controlling UEP using a direct stability program, e.g., the TEF [31], for a given disturbance.
3. Find the Jacobian and the Hessian matrices at the UEP.
4. Conduct linear analysis to obtain the eigenvalues and eigenvectors.
5. Do similarity transformation to the 2^{nd} order terms.
6. Compute the $h2_r$, and the Γ coefficients.
7. Approximate the stable manifolds.
8. Project the stable manifolds to the angle subspace, and hence, display the shape of the approximated boundary.
9. Compute potential energy, and distance of the manifold from the SEP.

The overall approach is summarized in Figure 3.1. It also shows steps involved in the present methodology for the approximation of stable manifold of the controlling UEP which is a portion of the boundary.

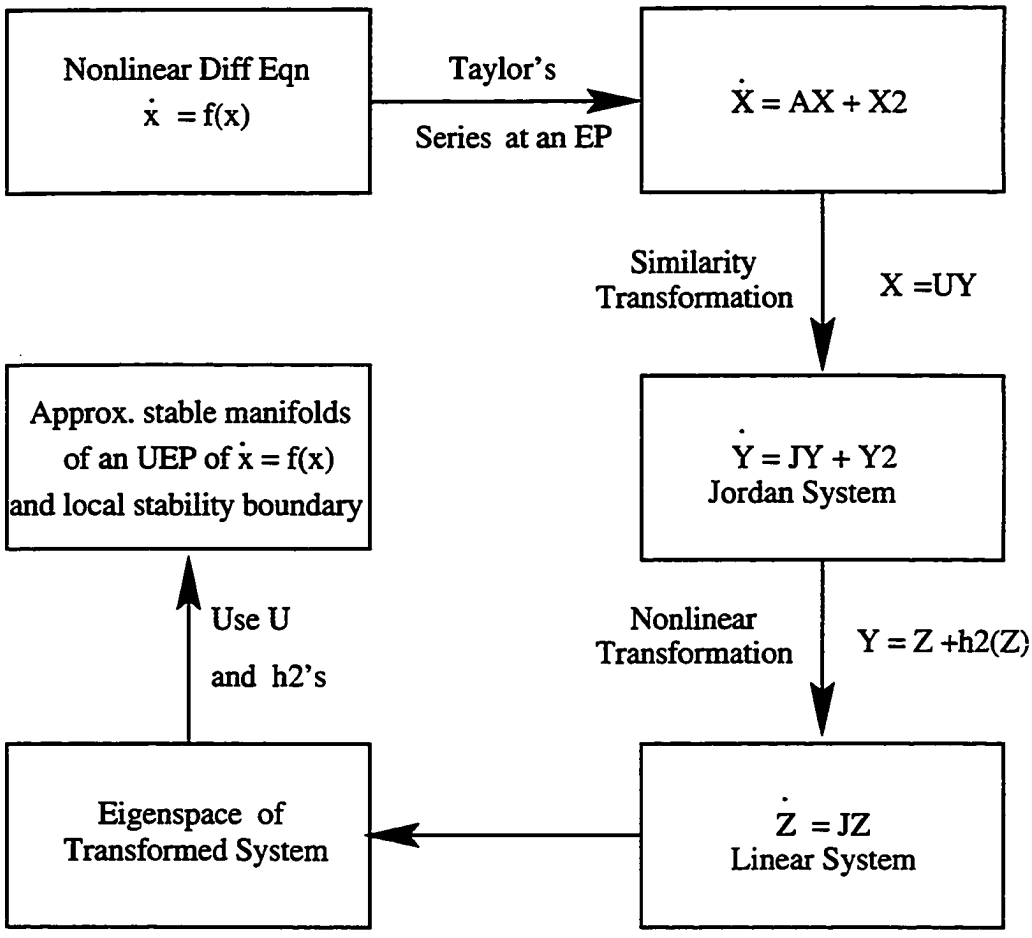

Figure 3.1: Solution steps

3.8 Summary

This chapter presents computational steps involved in approximating the stable manifold of a UEP of interest using the real normal form of vector fields. For any operating condition, we take points (3 points are taken here) on each linear manifold. For the purpose of computing energy and distance, the three points taken are for $\alpha = -1, \alpha = 0$, and $\alpha = 1$. $\alpha = 0$, is the controlling UEP itself. For each point (say $\alpha = 1$) on any manifold, we compute norm between this point, and the postfault SEP of the system. We compute potential energy at that point with respect to the postfault SEP. Note that for the computation of the energy and the norm, each point in the z-space is transformed back to x-space The next chapter provides numerical results to the concepts developed in this chapter.

4. NUMERICAL RESULTS

This chapter contains numerical results on different issues discussed in chapter 3. The results are presented on the following:

- The effect of fault location, and loading of critical generators, and number of lines opened to clear the fault, on the system eigenvalues, the interaction coefficients, $h2_r$ and the curvature coefficients, Γ.
- The shape of the manifold near the controlling UEP and the size of the region of stability.
- How the system trajectory approaches and leaves the boundary of the region of stability.
- The potential energy and the distance of the manifold from the postfault SEP.
- Effect of loading of the critical generators on the behavior of faulted trajectory.
- The behavior of equilibrium points when system is stressed.

4.1 11 Generator Test System

An 11 generator test system is used in this work. The 11 generator system comprises 55 buses and 183 lines [32]. Figure 4.1 provides a one-line diagram of the

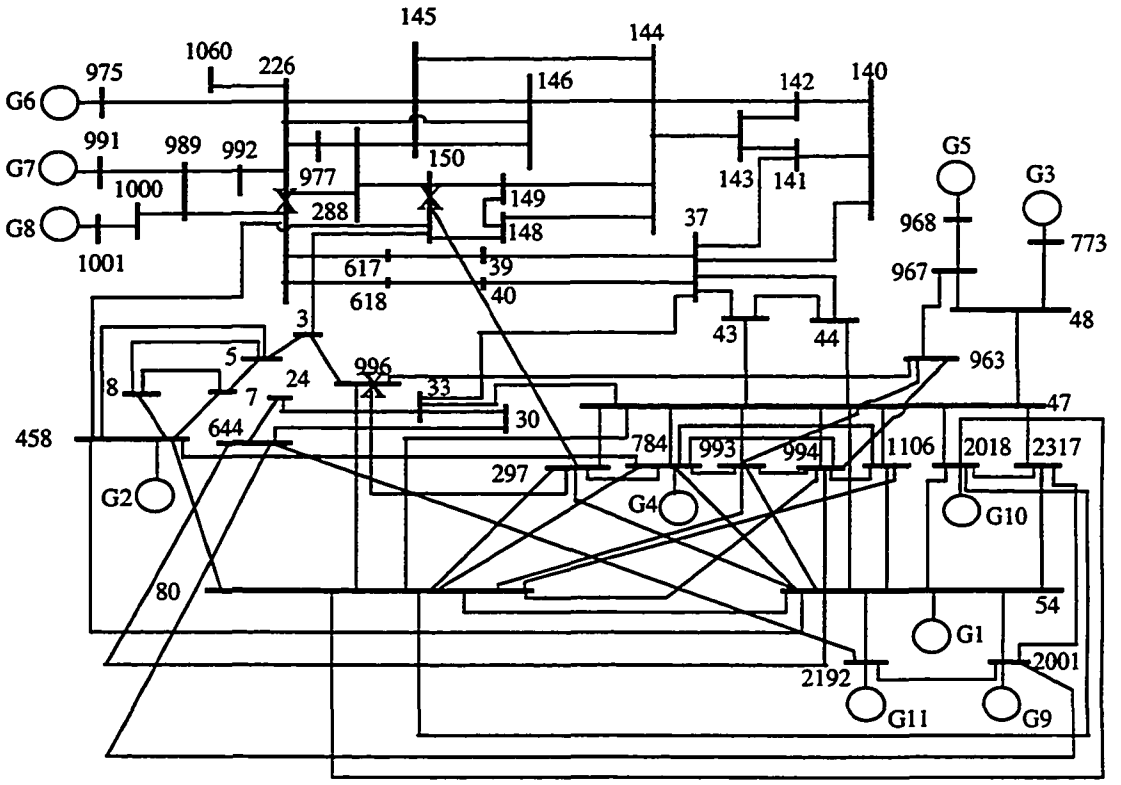

Figure 4.1: One-line diagram of 11 generator test system

11 generator test system. Fault locations are marked with 'X' in Figure 4.1. Results for three disturbances are given here:

- A three-phase fault at bus # 226, cleared at 0.068 second by opening lines 226-145, 144-145, 146-226, and 144-146.
- A three-phase fault at bus # 996, cleared at 0.068 second by opening lines 3-996 (2 lines), 297-996 (3 lines).
- A three-phase fault at bus # 150, cleared at 0.068 second by opening lines 150-458, 150-288, 150-3 (2 lines), and 150-297. and 226-145.

4.2 Simulation of Stress in a System

A power system can become stressed in a variety of ways. They are: heavier loading of some generators, heavier loading of some portion of the transmission network, and when it is subjected to severe faults. Stress also depends on the location of fault and the postfault network configurations. This dissertation considers the stress due to fault location, loading of some generators and the post fault system network. In this simulation, Case2 is more stressed than Case1 and Case3 is more than Case2 and so on.

Table 4.1 contains generations for different operating conditions. This Table corresponds to faults at bus # 996 and bus # 150. We see that the generation at generators 3 and 5 is increased to cause more stress in the system. For fault at bus # 226, the loading at the generators are different as the advanced machines are different. Table 4.2 contains generations at the critical generators for fault at bus #

Table 4.1: Loading at the generators, for faults at 996, 150

Gen #	Case1 MW	Case2 MW	Case3 MW	Case4 MW	Case5 MW
1	6357.5	6357.5	6357.5	6357.5	6357.5
2	1669.4	1669.4	1669.4	1669.4	1669.4
3	2149.2	2499.2	2699.2	2799.2	2949.2
4	500.0	500.0	500.0	500.0	500.0
5	2149.2	2499.2	2699.2	2799.2	2949.2
6	300.0	300.0	300.0	300.0	300.0
7	600.0	600.0	600.0	600.0	600.0
8	700.0	700.0	700.0	700.0	700.0
9	2827.6	2827.6	2827.6	2827.6	2827.6
10	5329.5	5329.5	5329.5	5329.5	5329.5
11	241880.0	240840.0	240410.0	240190.0	239860.0

Table 4.2: Generation at critical generators, fault at 226

Generator #	Case1 MW	Case 2 MW	Case3 MW	Case4 MW	Case 5 MW
6	200	300	100	350	150
7	500	600	200	650	250
8	600	700	1300	700	1350

226. Generations at the rest of the generators are the same as in Table 4.1 except for generator 11, which is a slack bus.

Generators where loading is increased are the "critical generators" whose loading greatly influences stability behavior. These generators are the advanced generators in the UEP. They are identified by a special procedure used in the TEF method of direct stability analysis. For a fault at bus # 226 the critical generators are generator numbers 6,7, and 8; for a fault at bus # 150, or at bus # 996, the critical generators are numbers 3 and 5.

For each of the above mentioned cases Taylor series expansion of the system equations is made at the controlling UEP, and real normal form transformation is performed.

4.3 UEP Angles and System Eigenvalues

4.3.1 Effect of loading of critical generators

The UEPs for different loading cases for a fault at bus # 226 are presented in Table 4.3. For each case the advanced generators at the UEP are the same. It means that the same critical generators appear in all the UEPs but the magnitude of their angles in the UEP could be different for different cases. Eigenvalues are computed at the controlling UEP for a 3 phase fault at bus # 226 and are given in Table 4.4. Controlling UEPs for a fault at bus # 996 are given in Table 4.5. The angles presented in COI reference frame are given in degrees. Tables 4.4 and 4.6 show how real eigenvalues decrease with increased loading in the system.

4.3.2 Effect of fault location and postfault network

Tables 4.7 and 4.8 present controlling UEP angles and eigenvalues at this UEP for a 3 phase fault at bus # 150. CaseI corresponds to 3 lines removal and CaseII to 5 lines removal at fault clearing at same loading condition. It has been observed from these two Tables that for this 11 generator test system, the system is more affected by change in loading than by change of postfault system network.

Table 4.3: Controlling UEPs for a fault at bus 226

Generator	Case1 deg	Case2 deg	Case3 deg	Case4 deg	Case5 deg
1	28.962	27.123	26.934	25.292	23.463
2	26.444	24.261	24.023	22.031	19.758
3	44.952	42.504	42.257	40.163	37.811
4	21.005	18.808	18.576	16.613	14.389
5	42.484	40.054	39.808	37.717	35.365
6	145.251	122.636	112.507	111.217	91.347
7	149.599	125.054	116.655	112.621	94.286
8	147.909	123.014	132.349	109.635	108.839
9	-6.955	-7.192	-7.192	-7.569	-7.927
10	21.113	19.562	19.562	18.066	16.609
11	-6.509	-5.638	-5.638	-5.117	-4.615

4.4 Nonlinear Interaction Coefficients, $h2_r$

Here, one of the subjects of interest is the $h2_r(z)$ part of equation (2.11) in the normal form transformation. It represents the nonlinear interaction between the natural modes, and reflects the degree of "curvature" that exists in the normal form state space as compared to the original state space. This curvature is reflected in the invariant manifolds, i.e., the more stressed the power network, the more "curved" some of the manifolds will become. Since the manifolds form the boundary of the stability region, they present us with an opportunity to study the effect of stress (due to loading) on the behavior of the stability boundary, (approximated by the normal form transformation).

Table 4.4: Eigenvalues at the controlling UEP, fault at bus 226

Case1	Case2	Case3	Case4	Case5
2.381	1.845	1.829	1.488	-0.050+10.838j
-2.481	-1.945	-1.929	-1.588	-0.050-10.838j
-0.050+2.185j	-0.050+2.468j	-0.050+2.486j	-0.050+ 2.660j	-0.050+ 9.913j
-0.050-2.185j	-0.050-2.468j	-0.050 -2.486j	-0.050-2.660j	-0.050 -9.913j
-0.050+10.562j	-0.050+10.697j	-0.050+10.705j	-0.050+10.773j	1.108
-0.050-10.562j	-0.050-10.697j	-0.050-10.705j	-0.050-10.773j	-1.208
-0.050+ 9.653j	-0.050+ 9.782j	-0.050+9.788j	-0.050+ 9.852j	-0.050+2.832j
-0.050-9.653j	-0.050-9.782j	-0.050-9.788j	-0.050 -9.852j	-0.050-2.832j
-0.050+ 8.725j	-0.050+8.824j	-0.050+8.830j	-0.050+ 8.886j	-0.050+8.940j
-0.050-8.725j	-0.050-8.824j	-0.050-8.830j	-0.050 -8.886j	-0.050-8.940j
-0.050+8.528j	-0.050+8.676j	-0.050+8.683j	-0.050+ 8.758j	-0.050+8.829j
-0.050-8.528j	-0.050-8.676j	-0.050-8.683j	-0.050-8.758j	-0.050-8.829j
-0.050+7.439j	-0.050+7.512j	-0.050+7.517j	-0.050+6.209j	-0.050+7.606j
-0.050-7.439j	-0.050-7.512j	-0.050-7.517j	-0.050-6.209j	-0.050-7.606j
-0.050+7.118j	-0.050+7.332j	-0.050+7.190j	-0.050+6.421j	-0.050+6.276j
-0.050-7.118j	-0.050-7.332j	-0.050-7.190j	-0.050-6.421j	-0.050-6.276j
-0.050+6.006j	-0.050+6.131j	-0.050+6.137j	-0.050+7.562j	-0.050 +7.415j
-0.050-6.006j	-0.050-6.131j	-0.050-6.137j	-0.050-7.562j	-0.050-7.415j
-0.050+6.043j	-0.050+6.293j	-0.050+6.316j	-0.050+7.447j	-0.050+6.567j
-0.050-6.043j	-0.050-6.293j	-0.050-6.316j	-0.050-7.447j	-0.050-6.567j

Table 4.5: Controlling UEPs for a fault at 996

Generator	Case2 deg	Case3 deg	Case4 deg
1	71.941	62.091	54.971
2	66.927	58.826	52.327
3	98.383	93.289	87.846
4	64.458	56.032	49.317
5	96.251	91.175	85.783
6	73.459	66.497	60.791
7	75.252	68.383	62.727
8	73.568	66.629	60.928
9	11.791	6.299	2.959
10	63.243	51.632	44.045
11	-7.874	-6.921	-6.203

Table 4.6: λ at the controlling UEP, fault at 996

	Case2	Case3	Case4
1	2.165	-0.050 10.323j	-0.050+10.403j
2	-2.265	-0.050-10.323j	-0.050-10.403j
3	-0.050+10.269j	-0.050 +9.685j	-0.050+ 9.794j
4	-0.050-10.269j	-0.050 -9.685j	-0.050 -9.794j
5	-0.050 +9.542j	1.698	1.251
6	-0.050 -9.542j	-1.798	-1.351
7	-0.050 +3.087j	-0.050 +3.229j	-0.050 +3.338j
8	-0.050 -3.087j	-0.050 -3.229j	-0.050 -3.338j
9	-0.050 +5.229j	-0.050 +5.340j	-0.050 +5.470j
10	-0.050 -5.229j	-0.050 -5.340j	-0.050 -5.470j
11	-0.050 +6.246j	-0.050 +8.341j	-0.050 +8.474j
12	-0.050 -6.246j	-0.050 -8.341j	-0.050 -8.474j
13	-0.050 +8.174j	-0.050 +7.945j	-0.050 +7.979j
14	-0.050 -8.174j	-0.050 -7.945j	-0.050 -7.979j
15	-0.050 +7.912j	-0.050 +7.842j	-0.050 +7.899j
16	-0.050 -7.912j	-0.050 -7.842j	-0.050 -7.899j
17	-0.050 +7.809j	-0.050 +6.700j	-0.050 +6.964j
18	-0.050 -7.809j	-0.050 -6.700j	-0.050 -6.964j
19	-0.050 +6.952j	-0.050 +6.990j	-0.050 +7.018j
20	-0.050 -6.952j	-0.050 -6.990j	-0.050 -7.018j

Table 4.7: Effect of line removal on UEP

Generator	CaseI deg	CaseII deg
1	94.217	93.661
2	84.167	84.838
3	102.439	102.158
4	78.816	79.183
5	99.867	99.798
6	74.731	71.436
7	77.705	74.433
8	76.530	73.253
9	32.163	31.368
10	96.091	95.117
11	-9.729	-9.590

Table 4.8: Effect of line removal on λ

CaseI	CaseII
3.01 + 0.00j	3.03 + 0.00j
-3.11 + 0.00j	-3.13 + 0.00j
-0.05 + 10.36j	-0.05 + 10.37j
-0.05 - 10.36j	-0.05 - 10.37j
-0.05 + 9.51j	-0.05 +9.56j
-0.05 - 9.51j	-0.05 -9.56j
-0.05 + 2.92j	-0.05 + 2.43j
-0.05 - 2.92j	-0.05 - 2.43j
-0.05 + 4.23j	-0.05 + 4.31j
-0.05 - 4.23j	-0.05 - 4.31j
-0.05 + 5.09j	-0.05 + 4.96j
-0.05 - 5.09j	-0.05 - 4.96j
-0.05 + 6.83j	-0.05 + 6.81j
-0.05 - 6.83j	-0.05 - 6.81j
-0.05 + 8.25j	-0.05 + 8.25j
-0.05 - 8.25j	-0.05 - 8.25j
-0.05 + 7.88j	-0.05 + 7.89j
-0.05 - 7.88j	-0.05 - 7.89j
-0.05 + 7.81j	-0.05 + 7.79j
-0.05 - 7.81j	-0.05 - 7.79j

4.4.1 Effect of loading of critical generators

Table 4.9 shows a few of the $h2_r$ coefficients for the fault at bus # 226 case. The magnitude of $h2_r$ coefficient is indicative of the amount of the interaction coefficients caused by the stress in the system. Thus, more stressed the system becomes the greater the magnitude of $h2_r$; as is shown in columns 4-7 of Table 4.9. We note, however, that the increase in the magnitude of $h2_r$ is not uniform in all directions, as shown in the last column of Table 4.9. Thus, it appears that the more stressed the power system becomes, the more curved the boundary of the region of stability, as indicated by the size of the $h2_r$ coefficients. However, the curvature tends to increase in certain directions (see subsection 4.6.1).

4.5 Γ Coefficients

4.5.1 Effect of loading of critical generators

Tables 4.10 and 4.11 contain a few of the curvature coefficients Γ for a fault at bus # 226 and for a fault at bus # 996 for different conditions of stress (due to loading), respectively. From Tables 4.10 and 4.11 we see that Γ increases with increased stress. It is evident that the size of the curvature coefficient Γ is higher in the state variables corresponding to the advanced machines.

4.5.2 Effect of fault location and postfault network

Stress in the system is created by (1) shifting generation to the "advanced machines", (2) fault at different locations with varying durations and (3) removing more lines at fault clearing. But it has been observed that for the present test system, the

Table 4.9: A few $h2_r$ coefficients for a fault at bus 226

i	j	k	Case 1	Case 2	Case 3	Case 4	Case 5
1	1	1	0.054	-0.118	0.120	-0.202	0.001
1	1	2	0.100	0.214	0.219	-0.361	0.000
2	1	1	0.018	0.040	0.041	-0.069	0.000
2	1	2	-0.108	0.235	-0.241	0.403	-0.001
2	2	2	-0.050	-0.107	-0.109	0.180	0.000
2	2	4	0.042	0.064	0.064	-0.076	0.000
3	1	2	-0.166	0.193	-0.194	0.209	0.002
3	1	4	-0.020	0.080	-0.082	0.141	-0.001
3	2	4	-0.018	-0.069	-0.071	0.122	-0.002
3	3	3	-0.068	-0.048	-0.047	0.037	-0.006
3	4	4	-0.135	-0.096	-0.094	0.075	-0.005
3	9	9	-0.069	-0.060	-0.057	0.052	0.003
3	10	10	-0.071	-0.058	-0.060	0.054	0.003
4	1	1	0.032	0.046	0.046	-0.053	0.000
4	1	3	0.031	-0.099	0.101	-0.160	0.001
4	2	3	0.030	0.093	0.095	-0.147	0.001
4	3	4	0.135	0.096	0.094	-0.075	0.005
5	2	6	-0.033	-0.093	-0.097	0.290	0.000
5	5	6	0.001	0.001	-0.001	0.001	0.717
5	6	6	0.002	0.002	-0.002	0.002	0.117
5	6	8	-0.001	0.001	0.001	0.001	-0.052
6	2	5	0.033	0.092	0.096	-0.289	0.000
6	5	5	-0.001	-0.001	0.001	-0.001	0.140
6	5	6	-0.002	-0.002	0.002	-0.002	0.822
6	5	8	0.000	0.000	0.000	0.000	0.061
6	6	6	0.000	0.000	0.000	0.000	-0.359
6	6	8	0.000	0.000	0.000	0.000	0.094
7	5	5	-0.001	0.001	0.001	0.001	0.078
7	5	6	-0.002	0.002	0.002	0.002	0.241
7	5	7	-0.002	-0.002	0.002	-0.002	-0.964
7	5	8	-0.001	-0.001	0.001	-0.001	-0.163
7	6	6	-0.001	0.001	0.001	0.001	0.067
7	6	7	-0.001	-0.001	0.001	-0.001	-0.107
7	6	8	-0.002	-0.002	0.002	-0.002	-0.086
8	5	5	0.000	0.000	0.000	0.000	0.060
8	5	7	0.001	0.001	-0.001	0.001	0.409
8	5	8	0.001	0.001	-0.001	0.001	-0.619
8	6	7	0.001	0.001	-0.001	0.001	0.103

Table 4.9 (Continued)

i	j	k	Case 1	Case 2	Case 3	Case 4	Case 5
9	6	10	0.000	0.000	0.000	0.000	-0.164
9	7	15	0.000	0.000	0.000	0.000	0.081
9	8	16	0.000	0.000	0.000	0.000	-0.087
10	6	9	0.000	0.000	0.000	0.000	0.164
13	2	12	-0.035	-0.009	-0.009	0.112	0.000
14	2	11	0.031	0.008	0.008	-0.086	0.000
15	1	15	0.015	-0.037	0.061	-0.060	0.000
15	2	15	0.004	-0.017	-0.020	0.106	0.000
15	2	16	-0.010	-0.016	-0.018	-0.279	0.000
15	2	19	0.001	-0.001	0.002	-0.061	0.000
15	2	20	0.000	0.002	0.001	0.130	0.000
15	5	9	0.000	0.000	0.000	0.000	-0.115
15	5	10	0.000	0.000	0.000	0.000	0.098
15	15	19	0.001	0.002	-0.005	-0.189	0.000
15	15	20	-0.001	-0.003	-0.003	0.160	0.000
15	16	20	-0.002	-0.002	-0.004	0.439	0.000
16	2	15	0.009	0.017	0.020	0.273	0.000
16	14	15	0.000	0.000	0.000	-0.152	-0.004
16	15	19	0.001	-0.002	0.002	-0.350	0.000
16	15	20	0.004	0.001	0.003	0.423	0.000
16	16	19	-0.003	0.001	0.001	-0.745	0.000
16	16	20	0.000	0.001	-0.002	-0.262	0.000
17	2	9	0.186	0.055	-0.081	0.010	0.000
17	2	10	-0.230	-0.067	0.097	-0.013	0.000
17	2	15	0.001	0.059	-0.387	0.000	0.000
17	2	16	-0.002	-0.119	0.808	0.000	0.000
18	2	9	0.177	0.048	-0.075	0.012	0.000
18	2	15	0.003	0.104	-0.715	0.000	0.000
18	6	17	0.000	0.000	0.000	0.000	-0.138
18	16	17	0.000	0.000	0.000	0.001	0.129
19	2	18	0.005	0.008	0.133	0.000	0.000
19	2	19	0.011	0.483	0.835	0.022	0.000
19	2	20	-0.084	-1.641	-2.980	0.021	0.000
20	2	17	-0.005	-0.008	-0.132	0.000	0.000
20	2	19	0.083	1.605	2.919	-0.021	0.000
20	2	20	-0.003	-0.116	-0.200	-0.004	0.000
20	18	19	0.173	-0.175	-0.176	0.000	-0.002

Table 4.10: A few Γ_{ij} for fault at bus 226

i	j	Case1	Case2	Case3	Case4	Case5
1	3	0.010	0.007	0.007	0.005	0.001
1	4	0.020	0.014	0.013	0.010	0.002
2	4	0.022	0.015	0.015	0.011	0.002
2	9	0.011	0.009	0.009	0.008	0.007
2	10	0.011	0.009	0.009	0.008	0.007
3	3	0.010	0.007	0.007	0.005	0.002
3	4	0.022	0.015	0.014	0.011	0.002
3	9	0.011	0.009	0.009	0.008	0.007
3	10	0.011	0.009	0.009	0.008	0.007
4	3	0.010	0.006	0.006	0.004	0.002
4	4	0.022	0.015	0.014	0.011	0.002
4	9	0.011	0.009	0.009	0.008	0.007
4	10	0.011	0.009	0.009	0.008	0.007
5	10	0.011	0.009	0.009	0.008	0.007
6	1	0.007	0.021	0.021	0.042	0.000
6	2	0.006	0.018	0.018	0.035	0.000
6	3	0.012	0.005	0.005	0.001	0.001
6	4	0.015	0.007	0.007	0.002	0.001
6	5	0.003	0.002	0.002	0.001	0.101
6	6	0.003	0.002	0.002	0.001	0.082
6	10	0.010	0.007	0.007	0.006	0.004
6	17	0.006	0.004	0.004	0.004	-0.023
6	18	0.006	0.004	0.004	0.004	-0.023
6	19	-0.003	-0.005	-0.006	-0.012	-0.015
6	20	-0.003	-0.006	-0.007	-0.012	-0.014
7	1	0.006	0.019	0.020	0.040	0.000
7	2	0.006	0.016	0.017	0.034	0.000
7	3	0.012	0.005	0.005	0.000	0.001
7	4	0.015	0.007	0.007	0.002	0.001
7	5	0.003	0.002	0.002	0.001	0.100
7	6	0.003	0.002	0.002	0.001	0.081
7	15	-0.004	-0.008	-0.010	-0.009	0.002
7	16	-0.005	-0.008	-0.010	-0.009	0.002
7	17	0.006	0.004	0.004	0.004	-0.023
7	18	0.006	0.004	0.004	0.004	-0.023
7	19	-0.004	-0.006	-0.006	-0.012	-0.015
7	20	-0.004	-0.006	-0.006	-0.011	-0.015

Table 4.10 (Continued)

i	j	Case1	Case2	Case3	Case4	Case5
8	2	0.006	0.018	0.018	0.035	0.000
8	3	0.012	0.006	0.005	0.001	0.001
8	4	0.015	0.007	0.007	0.002	0.001
8	5	0.003	0.002	0.002	0.001	0.106
8	6	0.003	0.002	0.002	0.001	0.086
8	17	0.006	0.004	0.004	0.004	-0.022
8	18	0.006	0.004	0.004	0.004	-0.021
8	19	-0.004	-0.006	-0.006	-0.012	-0.015
8	20	-0.004	-0.006	-0.006	-0.012	-0.015
10	3	0.011	0.008	0.008	0.006	0.001
10	4	0.019	0.013	0.013	0.010	0.001
11	5	0.000	0.000	0.000	0.000	0.014
11	6	-0.001	-0.001	0.000	0.000	-0.011
12	5	0.000	0.000	0.000	0.000	0.017
12	6	-0.001	-0.001	-0.001	-0.001	-0.013
13	5	-0.002	-0.002	-0.002	-0.002	0.020
13	6	0.000	0.000	0.000	0.000	-0.016
14	1	-0.014	-0.012	-0.012	-0.005	0.000
14	2	0.013	0.012	0.012	0.005	-0.001
15	1	-0.015	-0.012	-0.012	-0.003	-0.003
15	2	0.014	0.011	0.011	0.004	-0.001
16	1	0.034	0.076	0.076	0.125	0.000
16	2	-0.032	-0.069	-0.069	-0.112	0.000
16	5	0.000	0.000	0.000	0.000	0.224
16	6	0.000	0.000	0.000	0.000	-0.197
17	1	0.031	0.071	0.073	0.120	0.000
17	2	-0.028	-0.064	-0.065	-0.107	0.000
17	5	0.000	0.000	0.000	0.000	0.222
17	6	0.000	0.000	0.000	0.000	-0.195
18	1	0.034	0.076	0.079	0.125	0.000
18	2	-0.031	-0.069	-0.071	-0.111	0.000
18	5	0.000	0.000	0.000	0.000	0.236
18	6	0.000	0.000	0.000	0.000	-0.207

Table 4.11: A few Γ_{ij} for fault at 996

i	j	Case2	Case3	Case4
1	5	-0.002	0.024	0.059
2	5	-0.001	0.019	0.052
3	5	-0.002	0.023	0.063
3	6	-0.002	0.020	0.052
4	5	-0.001	0.021	0.056
5	5	-0.002	0.023	0.062
5	6	-0.002	0.020	0.051
10	5	-0.002	0.026	0.060
10	6	-0.002	0.022	0.050
11	5	0.000	0.080	0.147
11	6	0.000	-0.073	-0.131
12	5	0.001	0.065	0.130
12	6	0.000	-0.058	-0.115
13	5	0.001	0.080	0.157
13	6	0.001	-0.072	-0.139
14	5	0.005	0.072	0.141
14	6	0.007	-0.065	-0.125
15	5	0.001	0.078	0.155
15	6	0.001	-0.070	-0.137
16	5	0.000	0.035	0.085
16	6	0.000	-0.031	-0.074
17	5	0.000	0.033	0.082
17	6	0.000	-0.029	-0.071
18	5	0.000	0.035	0.085
18	6	0.000	-0.031	-0.074
19	5	-0.001	0.040	0.068
19	6	-0.001	-0.036	-0.061
20	1	0.056	0.004	0.004
20	2	-0.052	0.004	0.004
20	5	-0.001	0.088	0.150
20	6	-0.001	-0.079	-0.134

effect of loading the generators has more effect on the $h2$ and Γ coefficients than the number of line clearing conditions.

4.6 Shape of Manifold Near the UEP and Size of the Region of Stability

Stable manifold of the controlling UEP in the x-space is computed from the linear stable manifold of the z-system of (2.12). This linear manifold is then transformed back to the y-space using the equation (2.11). As (2.11) is nonlinear (quadratic), the linear manifold in the z-space becomes parabolic in the y-space and also parabolic in the x-space as the transformation from y to x is linear. Thus, the stable manifold in the x-space is approximated up to 2^{nd} order using 2^{nd} order normal form transformation.

4.6.1 Effect of loading of critical generators

Figure 4.2 shows portion of the stability boundaries with the corresponding SEPs for a fault at bus # 996; three different loading cases are shown. The boundary has been projected to the angle subspace of machines 1, 2 and 3. In Figure 4.3 the same boundary is projected to the angle subspace of generators 3, 1 and 5. We clearly see that the boundaries are more curved in the advanced machines directions (here machine 3 and machine 5). Figure 4.4 depicts stability boundaries for a fault at bus # 150. As for the fault at bus # 996, it is clearly seen that the region of stability is reduced with the increase in system stress due to loading [33]. This is also true for the fault at bus # 150.

4.7 Trajectory Behavior Near the Boundary of the Region of Stability

Figure 4.5 shows how the postfault trajectory approaches the stability boundary depending on the clearing time. If the fault is cleared before the critical clearing the postfault trajectory returns to the SEP and it follows the unstable manifold within the region of attraction. In Figure 4.5, the trajectory leaves the region of attraction for a clearing time of 0.064s whereas it is stable for 0.048s clearing. Figures 4.6 and 4.7 display similar phenomenon in two dimensional subspace.

4.7.1 Behavior of system trajectory near the UEP

Figure 4.8 explains the behavior of the faulted trajectory near the UEP. Figure 4.8 corresponds to equivalent one machine connected to infinite bus system. Figure 4.8.a depicts phase portrait of the system. The faulted trajectory leaves the region of stability depending on the time of fault clearing. In other words, the trajectory leaves the region of the stability when the fault is cleared after the critical clearing time. It is clear in Figure 4.8.c that the unstable trajectory leaves the boundary and follows the unstable manifold of the UEP, and that the stable trajectory follows the stable manifold near the UEP and then unstable manifold inside the region of stability of the SEP.

4.7.2 How the faulted trajectory leaves the boundary

Figures 4.9 and 4.10 show the effect of loading on the behavior of trajectory. They show how the trajectory leaves the boundary at higher loading, for the same clearing time, and the same fault. The trajectories leave at different edges of the boundary when the faults are cleared after the critical clearing time.

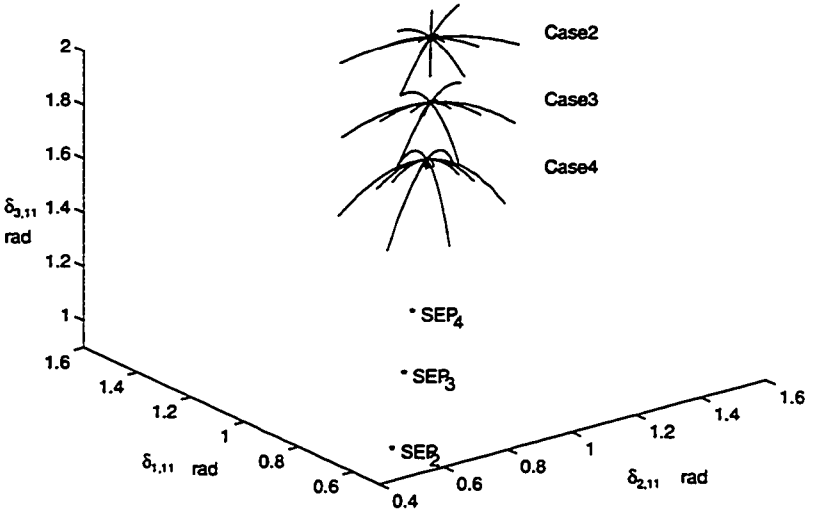

Figure 4.2: Fault at bus 996, boundaries for different stress conditions

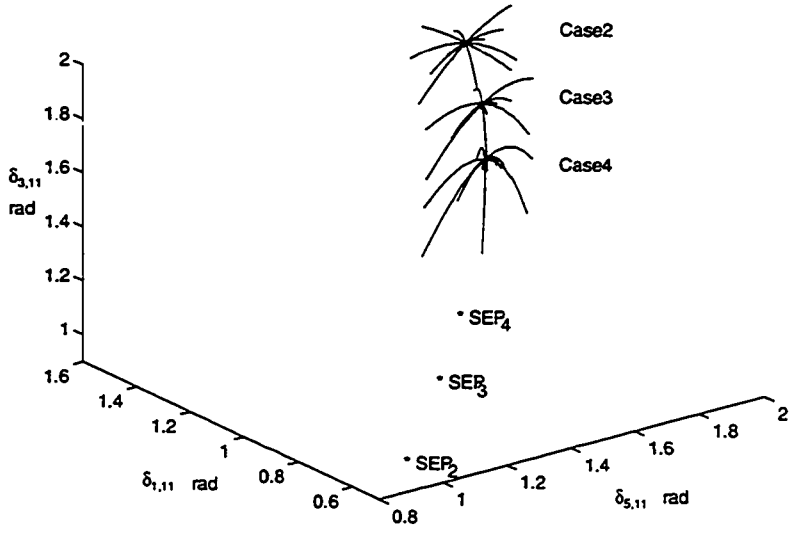

Figure 4.3: Fault at bus 996, boundaries for different stress conditions

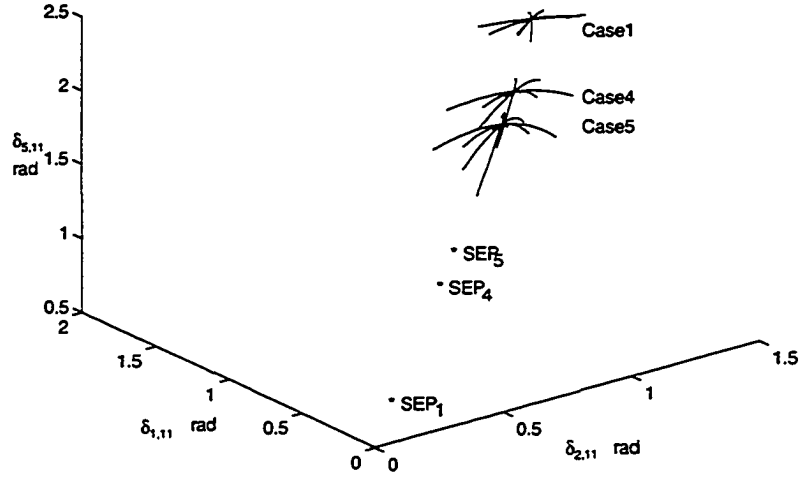

Figure 4.4: Fault at bus 150, boundaries for different stress conditions

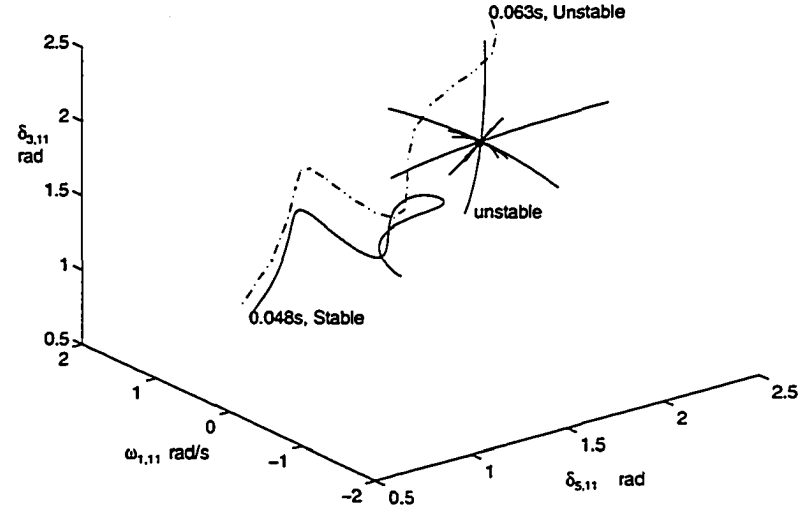

Figure 4.5: Trajectory near the UEP for a fault at bus 996 in 3 dimension

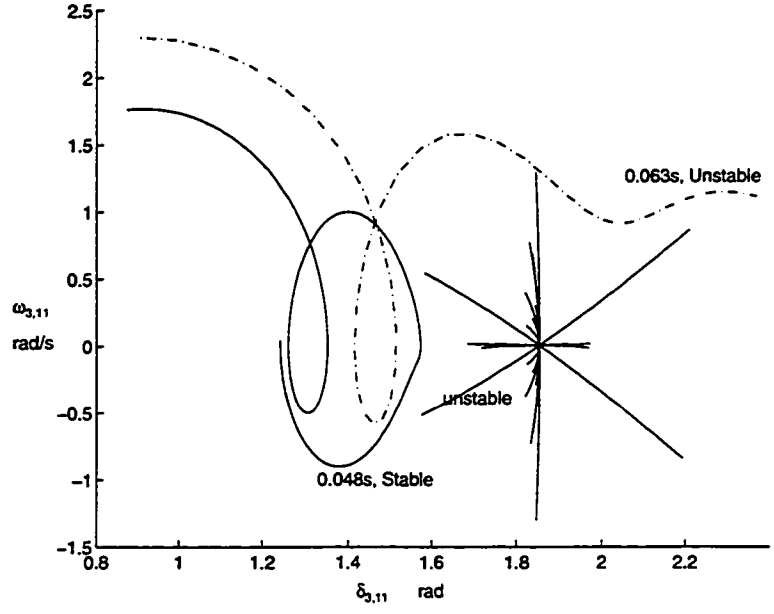

Figure 4.6: Trajectory near the UEP for a fault at 996 in 2 dimension (machine 3)

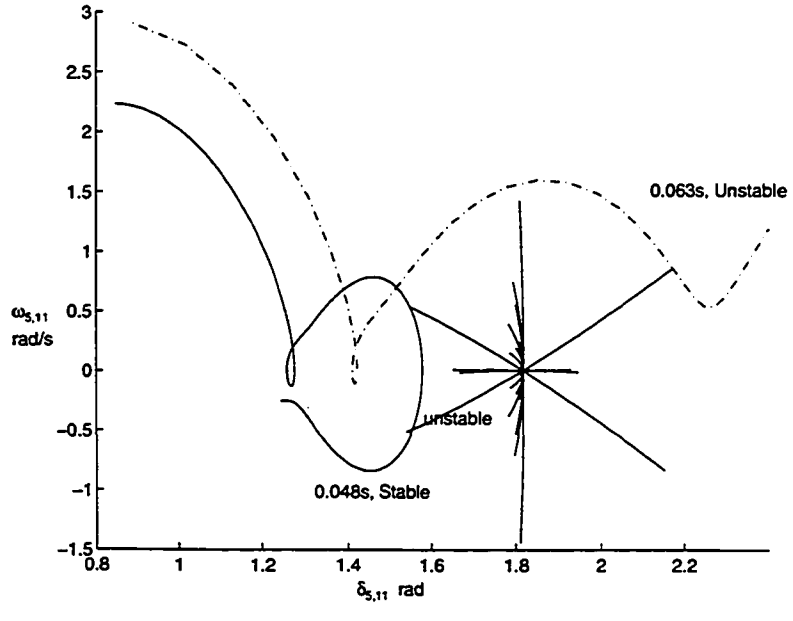

Figure 4.7: Trajectory near the UEP for a fault at 996 in 2 dimension (machine 5)

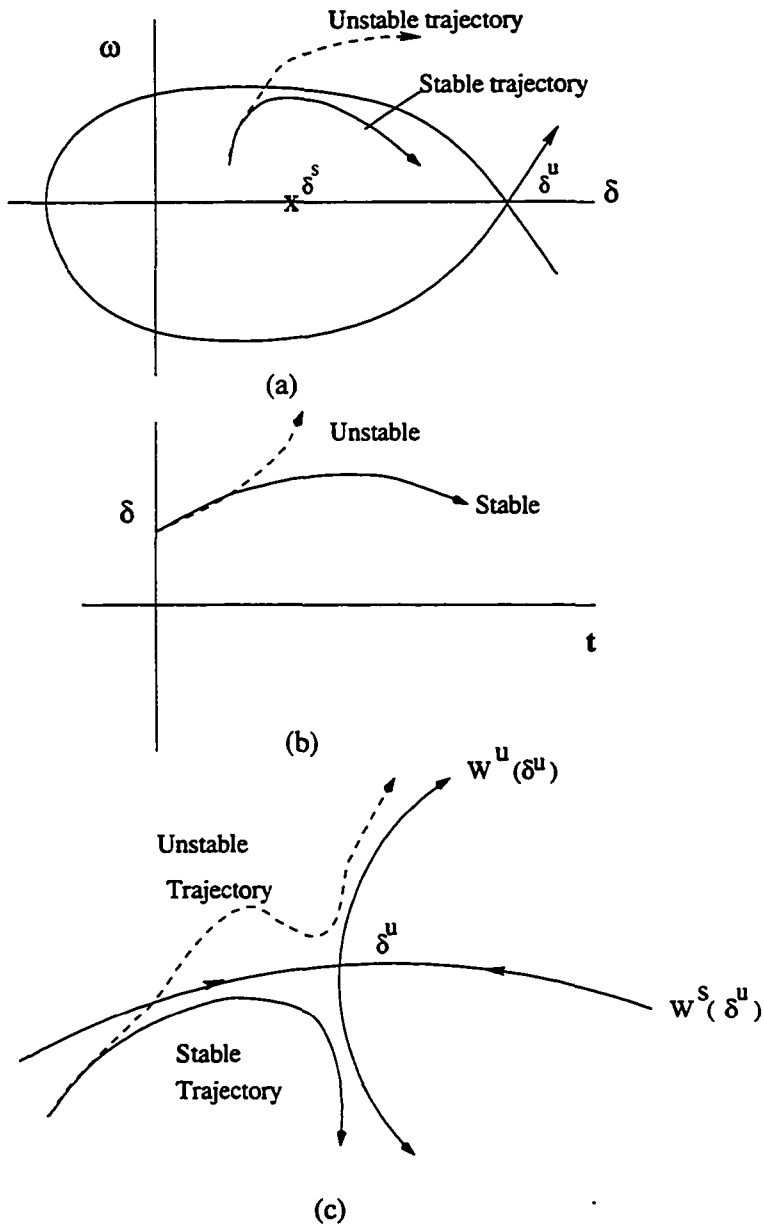

Figure 4.8: Trajectory near the UEP

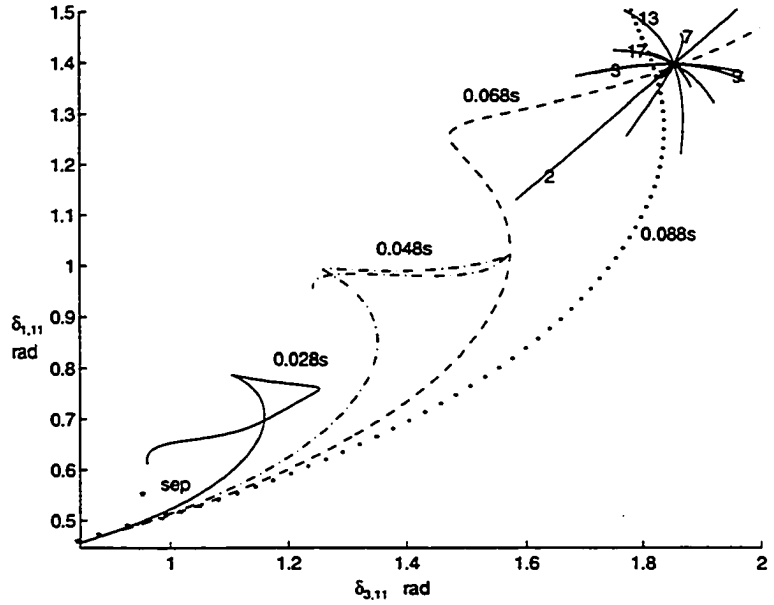

Figure 4.9: Faulted trajectories for a fault at bus 996, loading Case2

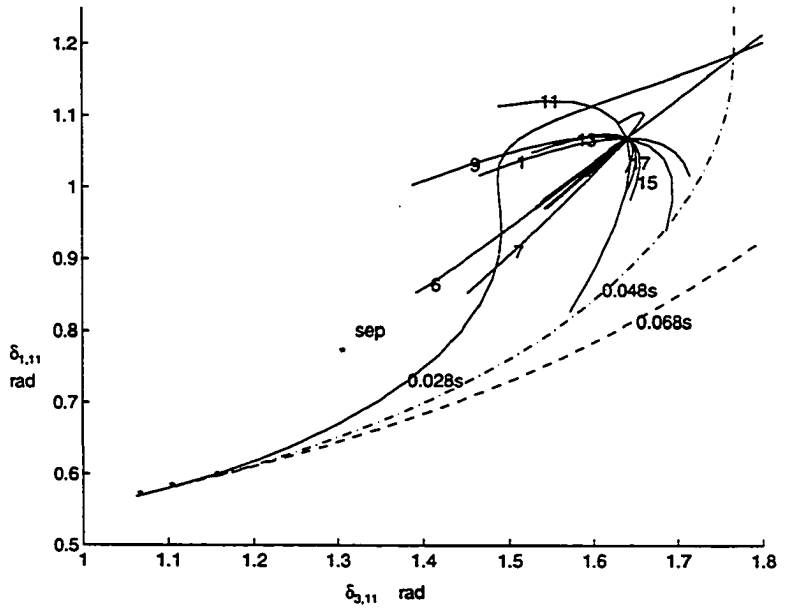

Figure 4.10: Faulted trajectories for a fault at bus 996, loading Case4

4.8 Potential Energy and Distance of Manifold from the Postfault SEP

4.8.1 Effect of loading of critical generators

The distance between a postfault SEP, θ^S and any point, θ on any manifold is given by the norm-2, defined as:

$$\sqrt{\sum_{i=1}^{N}(\theta(i)-\theta^S(i))^2} \tag{4.1}$$

where N is the dimension of the system. Norm-2 is also known as the Euclidean distance. For the computation of the energy and norm-2 we take a point on any stable eigenvector direction at a distance α from the UEP. Then that point is transformed to the y-space and then to the x-space, then potential energy and norm-2 are computed using (3.17) and (4.1).

Tables 4.12 and 4.13 are for Case2 and Case4 respectively for a fault at bus # 996. From this data, it is observed that the potential energy is almost constant at lower stress. In Table 4.12, the first row corresponds to unstable real eigenvalue and the second row corresponds to real stable eigenvalue for Case2. For Case4, the fifth row and sixth row of Table 4.13 correspond to real eigenvalues. The potential energy varies appreciably for a higher stress as given in Table 4.13 but the change is more along the manifold corresponding to real eigenvalues.

Reference [34] provides a graphical analysis of the potential energy surface around the UEP of a stressed power system. It has been shown that the potential energy surface around a UEP may be "very steep" in certain directions and "shallow" in other directions. The results presented in this chapter support the above mentioned observations.

Table 4.12: Potential energy and norm for a fault at bus 996, Case2

Potential Energy			Norm-2		
$\alpha = -1$	$\alpha = 0$	$\alpha = 1$	$\alpha = -1$	$\alpha = 0$	$\alpha = 1$
2.4016	2.6547	2.4375	2.2761	2.5209	3.1316
2.4135	2.6547	2.4603	2.2933	2.5209	3.1132
2.7467	2.6547	2.8571	2.5060	2.5209	2.5180
2.6379	2.6547	2.6374	2.7007	2.5209	2.7004
2.8184	2.6547	2.6035	2.5450	2.5209	2.4910
2.6523	2.6547	2.6543	2.7078	2.5209	2.7034
3.1635	2.6547	2.5188	2.4420	2.5209	2.5906
2.6453	2.6547	2.6557	2.6774	2.5209	2.6776
2.1115	2.6547	3.6745	2.5227	2.5209	2.4934
2.6651	2.6547	2.6500	2.6877	2.5209	2.6897
2.4358	2.6547	3.4456	2.4794	2.5209	2.5521
2.6845	2.6547	2.6763	2.6957	2.5209	2.7016
2.9596	2.6547	2.9479	2.4662	2.5209	2.5292
2.6464	2.6547	2.6464	2.6858	2.5209	2.6860
2.7265	2.6547	3.0691	2.5110	2.5209	2.5255
2.6499	2.6547	2.6477	2.7044	2.5209	2.7036
3.2439	2.6547	2.3844	2.5240	2.5209	2.4945
2.6382	2.6547	2.6436	2.6949	2.5209	2.6965
2.7884	2.6547	2.8302	2.5025	2.5209	2.5424
2.6519	2.6547	2.6516	2.7057	2.5209	2.7068

Table 4.13: Potential energy and norm for a fault at bus 996, Case4

Potential Energy			Norm-2		
$\alpha = -1$	$\alpha = 0$	$\alpha = 1$	$\alpha = -1$	$\alpha = 0$	$\alpha = 1$
0.2635	0.1176	0.3112	0.8743	0.9142	0.8887
0.1103	0.1176	0.1101	1.3265	0.9142	1.3263
0.1166	0.1176	0.1166	1.3390	0.9142	1.3424
0.2302	0.1176	0.1479	0.9306	0.9142	0.8772
-0.2978	0.1176	0.0548	2.0602	0.9142	0.5944
0.0544	0.1176	-0.2262	0.6419	0.9142	1.9998
0.2737	0.1176	0.4386	0.9263	0.9142	0.8609
0.1199	0.1176	0.1173	1.2831	0.9142	1.2795
0.6947	0.1176	0.1106	0.8434	0.9142	0.8761
0.1084	0.1176	0.1133	1.2956	0.9142	1.2957
0.5329	0.1176	0.4872	0.8226	0.9142	0.8707
0.1140	0.1176	0.1143	1.2992	0.9142	1.3017
0.4619	0.1176	0.2453	0.9119	0.9142	0.8783
0.1124	0.1176	0.1176	1.3298	0.9142	1.3314
0.1699	0.1176	0.4697	0.8661	0.9142	0.9037
0.1146	0.1176	0.1127	1.3241	0.9142	1.3236
0.5205	0.1176	0.2836	0.9319	0.9142	0.8776
0.1233	0.1176	0.1252	1.3401	0.9142	1.3281
0.2739	0.1176	0.2898	0.8951	0.9142	0.9344
0.1167	0.1176	0.1166	1.3397	0.9142	1.3418

4.8.2 Effect of fault location

Tables 4.14 and 4.15 contain potential energy and norm-2 for a 3 phase fault at bus # 150. For a fault at bus # 226 potential energy and norm-2 are tabulated in Tables 4.16 and 4.17.

Table 4.14: Potential energy and norm for a fault at bus 150, Case2

Potential Energy			Norm-2		
$\alpha = -1$	$\alpha = 0$	$\alpha = 1$	$\alpha = -1$	$\alpha = 0$	$\alpha = 1$
4.3944	4.3326	4.5507	2.9701	2.9834	2.9821
4.3156	4.3326	4.3149	3.1370	2.9834	3.1369
4.5139	4.3326	4.2618	3.0062	2.9834	2.9555
4.3302	4.3326	4.3315	3.1429	2.9834	3.1394
3.9856	4.3326	4.2003	2.7462	2.9834	3.5362
4.2179	4.3326	4.0008	3.5204	2.9834	2.7609
3.8563	4.3326	5.0268	3.0672	2.9834	2.9043
4.3043	4.3326	4.3040	3.1117	2.9834	3.1050
4.3600	4.3326	4.3600	3.1308	2.9834	3.1233
3.6667	4.3326	5.4718	2.9914	2.9834	2.9534
5.2470	4.3326	3.9705	3.0177	2.9834	2.9399
4.3525	4.3326	4.3632	3.1372	2.9834	3.1317
4.4844	4.3326	4.4780	3.0052	2.9834	2.9667
4.3257	4.3326	4.3262	3.1411	2.9834	3.1422
4.2589	4.3326	4.7619	2.9362	2.9834	3.0052
4.3295	4.3326	4.3314	3.1302	2.9834	3.1311
5.0848	4.3326	4.0706	2.9606	2.9834	2.9673
4.3162	4.3326	4.3225	3.1221	2.9834	3.1261
4.5799	4.3326	4.5757	2.9877	2.9834	2.9806
4.3221	4.3326	4.3222	3.1422	2.9834	3.1424

Table 4.15: Potential energy and norm for a fault at bus 150, Case5

Potential Energy			Norm-2		
$\alpha = -1$	$\alpha = 0$	$\alpha = 1$	$\alpha = -1$	$\alpha = 0$	$\alpha = 1$
0.4270	0.3157	0.5218	1.2443	1.2785	1.2623
0.3056	0.3157	0.3052	1.5982	1.2785	1.5978
0.3246	0.3157	0.4460	1.2454	1.2785	1.2956
0.3147	0.3157	0.3138	1.6103	1.2785	1.6121
0.0158	0.3157	0.2001	2.2348	1.2785	0.9736
0.0615	0.3157	0.2026	2.1918	1.2785	1.0086
0.7226	0.3157	0.3076	1.2459	1.2785	1.2699
0.3015	0.3157	0.3094	1.5308	1.2785	1.5383
0.1681	0.3157	1.0424	1.2541	1.2785	1.2179
0.3153	0.3157	0.3090	1.5701	1.2785	1.5713
0.6652	0.3157	0.6133	1.2650	1.2785	1.2039
0.3128	0.3157	0.3131	1.5820	1.2785	1.5801
0.2428	0.3157	0.7808	1.2222	1.2785	1.2622
0.3071	0.3157	0.3039	1.5890	1.2785	1.5828
0.5759	0.3157	0.5782	1.2772	1.2785	1.2699
0.3117	0.3157	0.3117	1.6094	1.2785	1.6097
0.7639	0.3157	0.4383	1.2978	1.2785	1.2472
0.3249	0.3157	0.3274	1.6112	1.2785	1.6016
0.4615	0.3157	0.4935	1.2567	1.2785	1.2998
0.3132	0.3157	0.3128	1.6096	1.2785	1.6116

Table 4.16: Potential energy and norm for a fault at bus 226, Case1

Potential Energy			Norm-2		
$\alpha = -1$	$\alpha = 0$	$\alpha = 1$	$\alpha = -1$	$\alpha = 0$	$\alpha = 1$
6.0090	5.9296	5.3753	3.7217	3.9803	4.4721
5.4059	5.9296	6.0129	4.4584	3.9803	3.7354
7.1591	5.9296	5.2585	4.2555	3.9803	3.7873
6.0339	5.9296	6.0800	4.1146	3.9803	4.1265
6.1431	5.9296	6.1205	3.9904	3.9803	3.9884
5.9508	5.9296	5.9509	4.1108	3.9803	4.1107
5.9661	5.9296	6.0637	3.9781	3.9803	3.9948
5.9432	5.9296	5.9426	4.1070	3.9803	4.1079
6.4244	5.9296	6.4114	4.0138	3.9803	3.9955
5.9924	5.9296	5.9924	4.1244	3.9803	4.1251
6.2983	5.9296	5.9472	3.9987	3.9803	3.9871
5.9589	5.9296	5.9610	4.1129	3.9803	4.1135
6.1603	5.9296	6.3154	3.9812	3.9803	4.0011
5.9526	5.9296	5.9515	4.1097	3.9803	4.1106
5.9288	5.9296	5.9288	4.0936	3.9803	4.0934
6.1772	5.9296	6.1731	3.9797	3.9803	3.9685
6.2307	5.9296	6.2591	3.9814	3.9803	4.0160
5.9726	5.9296	5.9724	4.1162	3.9803	4.1153
6.0651	5.9296	6.0905	3.9384	3.9803	4.0156
5.9289	5.9296	5.9286	4.0950	3.9803	4.0948

Table 4.17: Potential energy and norm for a fault at bus 226, Case5

Potential Energy			Norm-2		
$\alpha = -1$	$\alpha = 0$	$\alpha = 1$	$\alpha = -1$	$\alpha = 0$	$\alpha = 1$
0.2669	0.0712	0.2608	0.9251	0.9172	0.9229
0.0750	0.0712	0.0751	1.3554	0.9172	1.3555
0.1648	0.0712	0.1376	0.9344	0.9172	0.9157
0.0737	0.0712	0.0738	1.3564	0.9172	1.3535
-0.3531	0.0712	0.0325	2.0973	0.9172	0.5523
-0.2825	0.0712	0.0330	2.0299	0.9172	0.6020
0.5284	0.0712	0.1158	1.0917	0.9172	0.8278
0.0753	0.0712	0.0829	1.3162	0.9172	1.3039
0.5279	0.0712	0.5276	0.9249	0.9172	0.9468
0.0812	0.0712	0.0812	1.3601	0.9172	1.3614
0.2996	0.0712	0.2073	0.9326	0.9172	0.9215
0.0754	0.0712	0.0759	1.3531	0.9172	1.3556
0.3430	0.0712	0.3836	0.9245	0.9172	0.9467
0.0754	0.0712	0.0750	1.3529	0.9172	1.3613
0.3462	0.0712	0.3575	0.9177	0.9172	0.9566
0.0772	0.0712	0.0772	1.3529	0.9172	1.3521
0.3715	0.0712	0.3124	0.8923	0.9172	0.8802
0.0699	0.0712	0.0711	1.3196	0.9172	1.3261
0.2417	0.0712	0.2261	0.9385	0.9172	0.8659
0.0709	0.0712	0.0710	1.3308	0.9172	1.3305

4.9 Equilibrium Points When System is Stressed

Table 4.18 shows equilibrium points (EP)s for the three loading conditions. Columns 2 and 6 correspond to loading Case3 and columns 3 and 5 correspond to loading Case4 as given in Table 4.1. Generations at generators 3 and 5 are increased from 2699 MW each in Case3 to 2799 MW each in Case4. Generations in Case5 are 2899 MW each at generators 3 and 5. The generations at the rest are held constant except the generator 11, which is a slack bus. Eigenvalues at these EPs are computed and are used to classify these EPs as SEP or UEP. As we move from the 2^{nd} column to the 3^{rd} column, the angles in the SEPs increase; whereas from the 6^{th} column to the 4^{th} column the angles in the UEPs decrease. The point is that we clearly see that the SEP and UEP angles tend to move toward each other, and for higher loading the SEP and UEP may combine and the SEP disappears. In Table 4.18, the absence of SEP_5 appears to be due to the fact that it coalesced with the UEP_5.

Berggren et al [35] developed a conceptual framework for discussing equilibrium points, based on simple topological arguments. The authors analyzed certain fundamental properties of SEPs and UEPs in stressed power systems. In addition, they also show that some of the UEPs can disappear when the loading of the system increases.

4.10 Summary

This chapter presents numerical results of the proposed methodology to the 11 generator test system. The relation between the system stress due to loading and the boundary of the region of stability has been shown graphically. The shape of the

Table 4.18: Equilibrium points, fault at bus 996

Generator	SEP_3 deg	SEP_4 deg	UEP_5 deg	UEP_4 deg	UEP_3 deg
θ_1	34.4212	37.3540	46.9895	55.7975	62.0920
θ_2	30.8910	34.3678	44.7318	53.1944	58.8276
θ_3	62.2416	67.6700	80.9804	88.8224	93.2862
θ_4	27.4015	30.9128	41.4853	50.1995	56.0321
θ_5	60.3078	65.7344	78.9913	86.7519	91.1763
θ_6	41.4015	44.6653	54.0756	61.5868	66.4975
θ_7	43.4143	46.6889	56.0770	63.5236	68.3807
θ_8	41.5124	44.7932	54.2287	61.7297	66.6306
θ_9	-4.2309	-3.6969	-0.5210	3.2515	6.2993
θ_{10}	25.2713	27.4730	35.9139	44.7984	51.6313
θ_{11}	-3.9548	-4.3071	-5.3849	-6.2932	-6.9210

region of attraction of a power system for different degrees of stress has also been displayed. In addition, the behavior of the system trajectory near the UEP and as it leaves the boundary is studied. It is shown that when a faulted trajectory leaves the region of attraction, it follows the unstable manifold of the UEP.

It has been observed that the variation in magnitude of $h2_r$ with the increase in stress due to loading is not uniform in all the directions; it is more curved in the direction of the machine variables whose angles are advanced in the UEP. The real eigenvalue decreases with the increase in stress. The effect of stress due to more lines removal at fault clearing is found to have less effect than loading on $h2_r$, Γ.

It has been demonstrated that the stability region shrinks with stress and that the SEP and UEP tend to come close to each other. At higher stress the SEP and UEP may combine and the SEP disappears, as for Case5 in Table 4.18.

Potential energy on the approximate boundary has also been computed. It is

observed that the potential energy is almost constant in all directions around the UEP at lower stress condition but at higher stress it tends to change. It changes appreciably along the directions of the manifolds associated with real eigenvalues.

5. MODE OF SYSTEM INSTABILITY

The three previous chapters presented the formulation, methodology and numerical results of approximating stability boundary around the controlling UEP using the real normal forms of vector fields. This chapter will examine how this approximate boundary can be used to study machine separation from the system, when instability occurs.

5.1 Display of Trajectory to the Boundary

Chapter 4 contains numerical results of the approximate stability boundary around the controlling UEP for different operating conditions. Figures 4.9 and 4.10 show how trajectories behave near the UEP. They also show that the postfault system trajectories leave at different edges of the boundary for different clearing times, if any trajectory leaves the boundary. We now study this behavior to see if it can help explain the mode of machine separation from the system.

The postfault system can be written as equation (2.5). The reduced admittance matrix of the postfault system is obtained by running TEFV3.0 [31], a direct stability program. This system is integrated using a Runge-Kutta routine [36]. The condition at fault clearing is taken as initial condition for the purpose of integration. These integration results are also compared with EPRI's ETMSP [37] solution, a time simu-

lation package for transient stability analysis. The next section discusses the scheme to explain the mode of system separation.

5.2 Mode of System Separation

The steps involved in studying the mode of system separation using the approximate boundary and postfault system trajectory are as follows.

1. First, the stability boundary around the UEP is drawn, as done earlier.
2. Each manifold of the boundary is labeled.
3. The postfault system is integrated using the integration routine mentioned in section 5.1.
4. These faulted trajectories are drawn to this boundary for different initial conditions (depending on the fault clearing times).
5. The boundary is projected to a 2 dimensional angle subspace to show how the faulted trajectories cross the boundary, and the postfault trajectories are also projected to this angle subspace with different initial conditions.

It is expected that the faulted trajectories will leave the stability boundary at different points depending on the initial conditions.

Figure 5.1 presents a representative result to show how the postfault system trajectories leave the stability boundary for different clearing times. This figure corresponds to a 3 phase fault at bus # 150 for a loading Case5. The stability boundary around the controlling UEP and the postfault system trajectories are projected to the angle subspace of machines 5 and 1. Not all the manifolds are labeled in this

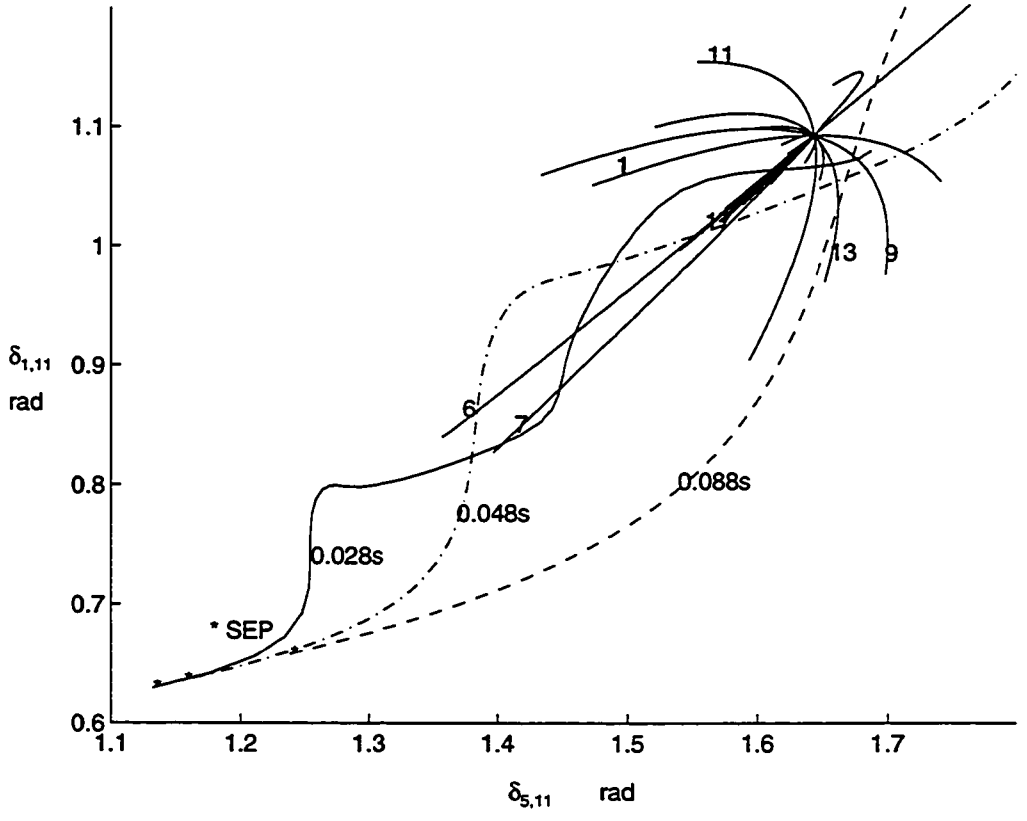

Figure 5.1: Faulted trajectories for different clearing times

figure in order that the figure may not be crowded. Note that, in this dissertation, the angles in the figures are given in radians. It is clearly seen the trajectories leave the boundary at different edges of the boundary depending on fault clearing time. For a clearing time of 0.028s, it leaves at manifold 7 and for a clearing time of 0.048s, it crosses boundary at manifold 6. As the clearing time increases, the trajectory appears to leave away from the UEP. The postfault trajectory for a fault clearing at 0.088s, probably leaves the boundary at manifold 11 (extending it) before it crosses manifold 13.

The crossing of the system trajectory at the edge of the boundary is also computed numerically. However, finding the exact crossing of the trajectory at the boundary is not always possible numerically. As observed in Figure 5.1, the problem is how to find the multidimensional point where it leaves the boundary when projected in 2 dimensional subspace. To overcome this computational problem, the following step is performed.

Assuming that the UEP is type-1 for the 11 generator test system, the edges of the boundary are represented by 19 stable manifolds. Many discrete points are taken on the manifolds. The postfault trajectory is then computed using an integration technique. At any instant of time, the Euclidean distance is computed between the points on the manifolds and the trajectory; the shortest distance is then taken. This distance shows how far is the trajectory from an edge of the boundary. It also identifies at, or close to, which manifold the faulted trajectory leaves the boundary. For an operating condition, the faulted trajectories, its minimum distance from a manifold and the identification of the manifold will be presented in Tables 5.1, 5.2, 5.3, and 5.4.

Table 5.1: Fault at bus 996, Case4, $t^{cl} = 0.028s$, only angle components

$\delta_{1,11}$ deg	$\delta_{2,11}$ deg	$\delta_{3,11}$ deg	$\delta_{4,11}$ deg	$\delta_{5,11}$ deg	$\delta_{6,11}$ deg	$\delta_{7,11}$ deg	$\delta_{8,11}$ deg	$\delta_{9,11}$ deg	$\delta_{10,11}$ deg	Dist. rad	#
32.38	30.99	60.37	24.96	58.09	41.64	43.71	41.79	-2.81	23.76	0.84	6
33.22	32.85	63.02	26.86	61.49	41.92	43.93	42.08	-2.78	23.97	0.77	6
34.16	34.49	65.76	28.85	64.91	42.21	44.17	42.38	-2.74	24.24	0.70	6
35.26	35.92	68.52	30.91	68.15	42.53	44.44	42.71	-2.66	24.64	0.63	6
36.53	37.16	71.25	32.99	71.08	42.92	44.78	43.10	-2.54	25.20	0.57	6
37.99	38.25	73.88	35.03	73.59	43.39	45.19	43.56	-2.35	25.96	0.51	6
39.62	39.24	76.36	36.99	75.65	43.96	45.69	44.12	-2.08	26.94	0.46	6
41.40	40.19	78.60	38.82	77.27	44.63	46.30	44.78	-1.71	28.18	0.41	6
43.29	41.15	80.56	40.48	78.47	45.43	47.02	45.55	-1.22	29.68	0.36	6
45.25	42.18	82.16	41.95	79.33	46.35	47.88	46.45	-0.61	31.43	0.31	6
47.22	43.31	83.39	43.21	79.95	47.40	48.86	47.47	0.15	33.42	0.27	6
49.15	44.54	84.22	44.27	80.42	48.56	49.97	48.60	1.05	35.63	0.22	6
51.00	45.88	84.69	45.17	80.83	49.84	51.21	49.86	2.09	38.00	0.19	6
52.72	47.30	84.86	45.95	81.25	51.23	52.58	51.23	3.27	40.49	0.18	6
54.29	48.76	84.80	46.65	81.72	52.72	54.07	52.71	4.57	43.02	0.18	6
55.69	50.22	84.64	47.34	82.29	54.29	55.66	54.27	5.96	45.53	0.18	6
56.93	51.63	84.51	48.06	82.94	55.93	57.35	55.91	7.41	47.96	0.18	6
58.01	52.94	84.53	48.85	83.69	57.63	59.12	57.62	8.89	50.22	0.19	6
58.96	54.12	84.82	49.74	84.51	59.37	60.95	59.38	10.34	52.26	0.18	10
59.80	55.16	85.47	50.73	85.40	61.14	62.82	61.17	11.73	54.03	0.17	9
60.58	56.06	86.52	51.83	86.36	62.92	64.71	62.98	13.01	55.48	0.12	9
61.34	56.84	87.96	53.00	87.39	64.69	66.61	64.79	14.13	56.59	0.09	9
62.10	57.55	89.75	54.22	88.54	66.46	68.50	66.59	15.06	57.36	0.09	9
62.89	58.24	91.81	55.48	89.82	68.19	70.35	68.37	15.74	57.79	0.12	9
63.73	58.97	94.05	56.75	91.29	69.90	72.16	70.11	16.17	57.92	0.17	6
64.64	59.82	96.37	58.02	92.96	71.56	73.91	71.82	16.33	57.80	0.15	6
65.62	60.84	98.67	59.30	94.85	73.18	75.60	73.47	16.20	57.48	0.14	6
66.66	62.08	100.89	60.60	96.95	74.76	77.21	75.07	15.81	57.05	0.13	6
67.76	63.58	103.00	61.96	99.24	76.30	78.75	76.62	15.18	56.58	0.13	6
68.91	65.33	104.98	63.40	101.65	77.79	80.23	78.12	14.34	56.16	0.14	6
70.10	67.34	106.86	64.96	104.14	79.25	81.64	79.57	13.36	55.88	0.17	6
71.32	69.55	108.67	66.66	106.64	80.67	82.99	80.99	12.31	55.82	0.19	6
72.60	71.93	110.46	68.52	109.07	82.07	84.29	82.36	11.28	56.04	0.22	6
73.93	74.41	112.29	70.53	111.39	83.46	85.57	83.72	10.34	56.62	0.25	6
75.35	76.92	114.21	72.67	113.56	84.84	86.82	85.06	9.60	57.58	0.27	6
76.87	79.39	116.25	74.92	115.59	86.21	88.07	86.40	9.14	58.96	0.29	6
78.53	81.77	118.42	77.25	117.48	87.60	89.33	87.74	9.05	60.77	0.31	6
80.38	84.02	120.73	79.59	119.28	89.00	90.61	89.10	9.37	63.03	0.31	6
82.45	86.11	123.16	81.93	121.06	90.43	91.93	90.48	10.17	65.71	0.30	6
84.77	88.05	125.70	84.23	122.90	91.88	93.31	91.90	11.45	68.82	0.29	6
87.39	89.86	128.33	86.50	124.88	93.38	94.74	93.38	13.23	72.34	0.26	6
90.34	91.60	131.04	88.75	127.09	94.92	96.24	94.91	15.48	76.26	0.23	6
97.36	95.17	136.74	93.44	132.49	98.20	99.50	98.19	21.24	85.28	0.24	6

Table 5.2: Fault at bus 996, Case4, $t^{cl} = 0.028s$, angle and speed components

$\delta_{1,11}$ deg	$\delta_{2,11}$ deg	$\delta_{3,11}$ deg	$\delta_{4,11}$ deg	$\delta_{5,11}$ deg	$\delta_{6,11}$ deg	$\delta_{7,11}$ deg	$\delta_{8,11}$ deg	$\delta_{9,11}$ deg	$\delta_{10,11}$ deg	Dist. rad	#
32.38	30.99	60.37	24.96	58.09	41.64	43.71	41.79	-2.81	23.76	2.12	6
33.22	32.85	63.02	26.86	61.49	41.92	43.93	42.08	-2.78	23.97	2.13	6
34.16	34.49	65.76	28.85	64.91	42.21	44.17	42.38	-2.74	24.24	2.08	6
35.26	35.92	68.52	30.91	68.15	42.53	44.44	42.71	-2.66	24.64	1.99	6
36.53	37.16	71.25	32.99	71.08	42.92	44.78	43.10	-2.54	25.20	1.86	6
37.99	38.25	73.88	35.03	73.59	43.39	45.19	43.56	-2.35	25.96	1.73	6
39.62	39.24	76.36	36.99	75.65	43.96	45.69	44.12	-2.08	26.94	1.60	6
41.40	40.19	78.60	38.82	77.27	44.63	46.30	44.78	-1.71	28.18	1.49	6
43.29	41.15	80.56	40.48	78.47	45.43	47.02	45.55	-1.22	29.68	1.42	6
45.25	42.18	82.16	41.95	79.33	46.35	47.88	46.45	-0.61	31.43	1.40	6
47.22	43.31	83.39	43.21	79.95	47.40	48.86	47.47	0.15	33.42	1.41	6
49.15	44.54	84.22	44.27	80.42	48.56	49.97	48.60	1.05	35.63	1.46	6
51.00	45.88	84.69	45.17	80.83	49.84	51.21	49.86	2.09	38.00	1.52	6
52.72	47.30	84.86	45.95	81.25	51.23	52.58	51.23	3.27	40.49	1.58	6
54.29	48.76	84.80	46.65	81.72	52.72	54.07	52.71	4.57	43.02	1.62	6
55.69	50.22	84.64	47.34	82.29	54.29	55.66	54.27	5.96	45.53	1.63	6
56.93	51.63	84.51	48.06	82.94	55.93	57.35	55.91	7.41	47.96	1.62	6
58.01	52.94	84.53	48.85	83.69	57.63	59.12	57.62	8.89	50.22	1.58	6
58.96	54.12	84.82	49.74	84.51	59.37	60.95	59.38	10.34	52.26	1.53	6
59.80	55.16	85.47	50.73	85.40	61.14	62.82	61.17	11.73	54.03	1.50	6
60.58	56.06	86.52	51.83	86.36	62.92	64.71	62.98	13.01	55.48	1.49	6
61.34	56.84	87.96	53.00	87.39	64.69	66.61	64.79	14.13	56.59	1.50	6
62.10	57.55	89.75	54.22	88.54	66.46	68.50	66.59	15.06	57.36	1.54	6
62.89	58.24	91.81	55.48	89.82	68.19	70.35	68.37	15.74	57.79	1.59	6
63.73	58.97	94.05	56.75	91.29	69.90	72.16	70.11	16.17	57.92	1.65	6
64.64	59.82	96.37	58.02	92.96	71.56	73.91	71.82	16.33	57.80	1.71	6
65.62	60.84	98.67	59.30	94.85	73.18	75.60	73.47	16.20	57.48	1.78	6
66.66	62.08	100.89	60.60	96.95	74.76	77.21	75.07	15.81	57.05	1.84	10
67.76	63.58	103.00	61.96	99.24	76.30	78.75	76.62	15.18	56.58	1.86	10
68.91	65.33	104.98	63.40	101.65	77.79	80.23	78.12	14.34	56.16	1.90	10
70.10	67.34	106.86	64.96	104.14	79.25	81.64	79.57	13.36	55.88	1.97	10
71.32	69.55	108.67	66.66	106.64	80.67	82.99	80.99	12.31	55.82	2.06	10
72.60	71.93	110.46	68.52	109.07	82.07	84.29	82.36	11.28	56.04	2.15	10
73.93	74.41	112.29	70.53	111.39	83.46	85.57	83.72	10.34	56.62	2.26	6
75.35	76.92	114.21	72.67	113.56	84.84	86.82	85.06	9.60	57.58	2.33	6
76.87	79.39	116.25	74.92	115.59	86.21	88.07	86.40	9.14	58.96	2.41	6
78.53	81.77	118.42	77.25	117.48	87.60	89.33	87.74	9.05	60.77	2.53	6
80.38	84.02	120.73	79.59	119.28	89.00	90.61	89.10	9.37	63.03	2.68	6
82.45	86.11	123.16	81.93	121.06	90.43	91.93	90.48	10.17	65.71	2.86	6
84.77	88.05	125.70	84.23	122.90	91.88	93.31	91.90	11.45	68.82	3.08	6
87.39	89.86	128.33	86.50	124.88	93.38	94.74	93.38	13.23	72.34	3.34	6
90.34	91.60	131.04	88.75	127.09	94.92	96.24	94.91	15.48	76.26	3.63	18
97.36	95.17	136.74	93.44	132.49	98.20	99.50	98.19	21.24	85.28	4.28	18

Table 5.3: Fault at bus 996, Case4, $t^{cl} = 0.088s$, only angle components

$\delta_{1,11}$ deg	$\delta_{2,11}$ deg	$\delta_{3,11}$ deg	$\delta_{4,11}$ deg	$\delta_{5,11}$ deg	$\delta_{6,11}$ deg	$\delta_{7,11}$ deg	$\delta_{8,11}$ deg	$\delta_{9,11}$ deg	$\delta_{10,11}$ deg	Dist rad	#
34.83	37.03	68.40	30.67	68.36	42.50	44.42	42.70	-2.73	24.36	0.63	6
37.44	42.93	76.47	36.45	78.38	43.43	45.19	43.67	-2.62	25.10	0.49	6
40.38	48.39	84.41	42.23	87.62	44.50	46.08	44.78	-2.42	26.14	0.47	6
43.74	53.34	92.15	47.96	95.82	45.79	47.18	46.08	-2.10	27.58	0.50	9
47.60	57.77	99.64	53.58	102.90	47.34	48.53	47.63	-1.61	29.55	0.43	9
51.94	61.73	106.81	59.02	108.88	49.21	50.19	49.48	-0.91	32.12	0.47	9
56.75	65.29	113.62	64.23	113.89	51.43	52.19	51.66	0.05	35.37	0.57	9
61.99	68.55	120.00	69.17	118.09	54.03	54.56	54.20	1.31	39.34	0.70	9
67.59	71.63	125.87	73.82	121.71	57.01	57.35	57.12	2.91	44.06	0.82	6
73.50	74.69	131.20	78.20	124.96	60.39	60.55	60.42	4.89	49.54	0.81	6
79.65	77.87	135.95	82.35	128.06	64.16	64.17	64.11	7.28	55.78	0.77	6
86.00	81.30	140.11	86.36	131.23	68.31	68.23	68.18	10.09	62.78	0.72	6
92.53	85.13	143.74	90.33	134.63	72.84	72.71	72.64	13.35	70.50	0.65	6
99.24	89.46	146.92	94.42	138.41	77.74	77.62	77.49	17.05	78.94	0.58	6
106.15	94.39	149.82	98.79	142.67	83.00	82.93	82.72	21.20	88.11	0.55	6
113.34	99.98	152.68	103.61	147.45	88.62	88.65	88.34	25.81	98.01	0.69	6
120.90	106.28	155.79	109.06	152.81	94.61	94.76	94.34	30.89	108.71	0.95	6
128.96	113.32	159.51	115.31	158.76	100.96	101.27	100.75	36.48	120.26	1.30	6
137.70	121.14	164.24	122.52	165.36	107.71	108.17	107.58	42.63	132.78	1.70	6
147.33	129.78	170.37	130.83	172.70	114.89	115.47	114.85	49.42	146.43	2.15	6
158.12	139.30	178.29	140.39	180.95	122.54	123.22	122.62	57.00	161.36	2.66	6
170.36	149.80	188.31	151.34	190.35	130.74	131.45	130.95	65.55	177.79	3.24	6
184.37	161.45	200.71	163.83	201.24	139.57	140.23	139.90	75.34	195.90	3.90	6
200.46	174.45	215.64	178.08	214.04	149.15	149.65	149.59	86.75	215.85	4.64	6
218.94	189.08	233.20	194.30	229.18	159.59	159.83	160.13	100.32	237.69	5.49	6
240.01	205.65	253.40	212.74	247.09	171.05	170.91	171.66	116.80	261.32	6.44	6
263.72	224.50	276.10	233.65	268.10	183.70	183.05	184.35	137.22	286.42	7.51	6
289.88	245.91	301.11	257.19	292.34	197.69	196.40	198.34	163.00	312.50	8.71	6
318.04	270.09	328.08	283.42	319.68	213.16	211.13	213.78	195.83	338.90	10.04	6
347.53	297.06	356.66	312.20	349.72	230.21	227.35	230.76	237.22	364.96	11.51	6
377.59	326.69	386.48	343.21	381.85	248.91	245.18	249.35	287.32	390.12	13.09	6
407.55	358.65	417.30	375.98	415.42	269.22	264.63	269.51	343.67	414.08	14.77	6
437.01	392.54	449.11	409.98	449.92	291.05	285.66	291.15	402.02	436.95	16.52	6
465.98	427.95	482.08	444.77	485.08	314.18	308.13	314.05	459.45	459.34	18.31	6
494.84	464.70	516.65	480.14	520.96	338.37	331.87	337.99	516.61	482.35	20.14	6
524.33	502.87	553.40	516.16	557.87	363.38	356.69	362.72	576.30	507.37	22.05	6
555.43	542.78	592.85	553.09	596.21	389.01	382.45	388.06	640.35	535.85	24.07	6
589.08	584.85	635.16	591.30	636.21	415.08	409.02	413.86	707.36	568.92	26.22	6
625.92	629.29	679.90	631.02	677.78	441.40	436.20	439.94	774.28	607.06	28.47	6
666.00	675.97	726.06	672.24	720.49	467.74	463.77	466.09	840.77	649.84	30.79	6
753.67	773.91	818.47	758.47	807.56	519.69	519.17	517.89	988.16	743.89	35.71	6

Table 5.4: Fault at bus 996, Case4, $t^{cl} = 0.088s$, both angle and speed components

$\delta_{1,11}$ deg	$\delta_{2,11}$ deg	$\delta_{3,11}$ deg	$\delta_{4,11}$ deg	$\delta_{5,11}$ deg	$\delta_{6,11}$ deg	$\delta_{7,11}$ deg	$\delta_{8,11}$ deg	$\delta_{9,11}$ deg	$\delta_{10,11}$ deg	Dist rad	#
34.83	37.03	68.40	30.67	68.36	42.50	44.42	42.70	-2.73	24.36	6.03	10
37.44	42.93	76.47	36.45	78.38	43.43	45.19	43.67	-2.62	25.10	5.84	10
40.38	48.39	84.41	42.23	87.62	44.50	46.08	44.78	-2.42	26.14	5.60	10
43.74	53.34	92.15	47.96	95.82	45.79	47.18	46.08	-2.10	27.58	5.39	10
47.60	57.77	99.64	53.58	102.90	47.34	48.53	47.63	-1.61	29.55	5.28	10
51.94	61.73	106.81	59.02	108.88	49.21	50.19	49.48	-0.91	32.12	5.20	6
56.75	65.29	113.62	64.23	113.89	51.43	52.19	51.66	0.05	35.37	5.12	6
61.99	68.55	120.00	69.17	118.09	54.03	54.56	54.20	1.31	39.34	5.15	6
67.59	71.63	125.87	73.82	121.71	57.01	57.35	57.12	2.91	44.06	5.28	6
73.50	74.69	131.20	78.20	124.96	60.39	60.55	60.42	4.89	49.54	5.51	6
79.65	77.87	135.95	82.35	128.06	64.16	64.17	64.11	7.28	55.78	5.82	6
86.00	81.30	140.11	86.36	131.23	68.31	68.23	68.18	10.09	62.78	6.21	6
92.53	85.13	143.74	90.33	134.63	72.84	72.71	72.64	13.35	70.50	6.68	6
99.24	89.46	146.92	94.42	138.41	77.74	77.62	77.49	17.05	78.94	7.22	6
106.15	94.39	149.82	98.79	142.67	83.00	82.93	82.72	21.20	88.11	7.84	6
113.34	99.98	152.68	103.61	147.45	88.62	88.65	88.34	25.81	98.01	8.55	6
120.90	106.28	155.79	109.06	152.81	94.61	94.76	94.34	30.89	108.71	9.35	6
128.96	113.32	159.51	115.31	158.76	100.96	101.27	100.75	36.48	120.26	10.26	18
137.70	121.14	164.24	122.52	165.36	107.71	108.17	107.58	42.63	132.78	11.32	18
147.33	129.78	170.37	130.83	172.70	114.89	115.47	114.85	49.42	146.43	12.57	18
158.12	139.30	178.29	140.39	180.95	122.54	123.22	122.62	57.00	161.36	14.07	18
170.36	149.80	188.31	151.34	190.35	130.74	131.45	130.95	65.55	177.79	15.84	18
184.37	161.45	200.71	163.83	201.24	139.57	140.23	139.90	75.34	195.90	17.93	18
200.46	174.45	215.64	178.08	214.04	149.15	149.65	149.59	86.75	215.85	20.35	18
218.94	189.08	233.20	194.30	229.18	159.59	159.83	160.13	100.32	237.69	23.08	18
240.01	205.65	253.40	212.74	247.09	171.05	170.91	171.66	116.80	261.32	26.12	18
263.72	224.50	276.10	233.65	268.10	183.70	183.05	184.35	137.22	286.42	29.41	18
289.88	245.91	301.11	257.19	292.34	197.69	196.40	198.34	163.00	312.50	32.94	18
318.04	270.09	328.08	283.42	319.68	213.16	211.13	213.78	195.83	338.90	36.67	18
347.53	297.06	356.66	312.20	349.72	230.21	227.35	230.76	237.22	364.96	40.48	18
377.59	326.69	386.48	343.21	381.85	248.91	245.18	249.35	287.32	390.12	43.95	18
407.55	358.65	417.30	375.98	415.42	269.22	264.63	269.51	343.67	414.08	46.44	18
437.01	392.54	449.11	409.98	449.92	291.05	285.66	291.15	402.02	436.95	47.91	18
465.98	427.95	482.08	444.77	485.08	314.18	308.13	314.05	459.45	459.34	49.19	18
494.84	464.70	516.65	480.14	520.96	338.37	331.87	337.99	516.61	482.35	51.18	18
524.33	502.87	553.40	516.16	557.87	363.38	356.69	362.72	576.30	507.37	54.17	18
555.43	542.78	592.85	553.09	596.21	389.01	382.45	388.06	640.35	535.85	57.71	18
589.08	584.85	635.16	591.30	636.21	415.08	409.02	413.86	707.36	568.92	60.99	18
625.92	629.29	679.90	631.02	677.78	441.40	436.20	439.94	774.28	607.06	63.82	18
666.00	675.97	726.06	672.24	720.49	467.74	463.77	466.09	840.77	649.84	66.66	18
753.67	773.91	818.47	758.47	807.56	519.69	519.17	517.89	988.16	743.89	73.30	18

Tables 5.1, 5.2, 5.3 and 5.4 present data for the postfault trajectories for a fault at bus # 996 and loading Case4 for different fault clearing times, t^{cl}. Tables 5.1 and 5.3 give only angle components of the trajectory and the boundary, whereas Tables 5.2, and 5.4 correspond to the computation which considers both angle and speed components of the trajectory and the boundary. In Table 5.1, it is seen that the faulted trajectory probably crosses manifold 9 (the Euclidean distance is minimum at 0.09) if only angles are taken into calculation. But, when both the speed and angle are considered, the minimum Euclidean distance shows that the trajectory leaves at manifold 6, as seen in Table 5.2. Manifold 6 corresponds to the stable real eigenvalue. For $t^{cl} = 0.088s$, the trajectory leaves or comes close to manifold 6 as shown in Tables 5.3 and 5.4. This shows that stability boundary only in angle subspace can be different from the stability boundary in the angle and speed space.

Chiang et al [38] also proposed the prediction of the unstable mode of a power system due to a fault cleared immediately after the critical clearing time using the unstable manifold of the controlling UEP. The unstable manifold of the controlling UEP is computed integrating the postfault system. But, the unstable manifold is computed in this dissertation using the real normal form of the vector fields.

5.3 Summary

This chapter presents a conceptual framework to study machine separation from the system using the approximate boundary and the postfault system trajectory. Both the graphical and numerical approaches are discussed. The concept is explained with examples and is applied to the 11 generator test system. It is observed that the trajectory leaves at different edges of the boundary depending on the clearing time,

as depicted in Figure 5.1. If the system trajectory leaves far away from the controlling UEP, the 2^{nd} approximation of the stability boundary may not be sufficient to implement this scheme to study the mode of system instability, as seen in Figure 5.1.

6. CONCLUSIONS AND SUGGESTIONS FOR FUTURE WORK

6.1 Conclusions

6.1.1 The goal

The goal of this dissertation is to understand and explain better the nonlinear phenomena of stressed power systems. Specific objectives are:

- To approximate the stability boundary of a SEP of a power system around the controlling UEP.
- To study the shape of the stability boundary and the region of attraction of the SEP.
- To analyze certain attributes of the stability boundary (e.g., curvature, potential energy etc.).
- To study how system trajectory approaches (or behaves near) the boundary.
- To study generators' separation from the system.

6.1.2 The approach

To address the above mentioned problems the following approach is followed:

- Real normal form formulation is proposed and implemented.
- To study the shape of the boundary under different stress conditions, a general computer program is developed. The program does the following tasks:
    1. Considers classical representation of the machines in a synchronous reference frame with the n^{th} machine taken as reference.
    2. Computes the Jacobian and Hessian matrices at the controlling UEP.
    3. Performs linear analysis of the system by computing the eigenvalues and eigenvectors.
    4. Does the real Jordan form transformation to linear, and second order terms.
    5. Applies real 2^{nd} order normal form transformation to the Jordan system.
    6. Displays the approximate stability boundary for different stress conditions to arbitrary 2 or 3 dimensional subspaces.
    7. Displays how the faulted trajectories approach the boundary.
    8. Calculates the norm-2 distance between the postfault SEP and points on the stable manifolds.
    9. Computes the potential energy on the stable manifolds.
- Used a test system under different conditions of system stress.
- Obtained results for certain conditions.

6.1.3 Important findings of this work

The important results obtained are:

- The relation between the system stress, due to loading at critical generators, and the boundary of the region of stability has been shown graphically.
- The shape of the region of attraction of postfault SEPs of a power system for different degrees of stress due to loading at the critical generators has also been displayed and analyzed.
- It has been found that the change in magnitude of nonlinear coefficients, $h2_r$ with increase in stress due to loading is not uniform in all the directions.
- The behavior of the system trajectory near the UEP and as it leaves the boundary is displayed. It is depicted that when a faulted trajectory leaves the region of attraction, it follows the unstable manifold of the UEP.
- The real eigenvalue of the system at the controlling UEP decreases with the increase in system stress.
- The effect of stress on eigenvalues, $h2_r$, Γ due to the removal of more lines at fault clearing is found to have less effect than the stress due to loading at least for this 11 generator test system.
- It has been shown that the stability region shrinks with stress, and that the SEP and UEP tend to come close to each other. At higher stress the SEP and UEP may combine and the SEP disappears.
- Potential energy on the approximate boundary is also computed. It is observed that except along the directions of the manifolds associated with real eigenvalues, the potential energy is almost constant in all directions around the UEP at lower stress but changes appreciably at higher stress.

- A conceptual framework for the study of the mode of system separation using the approximate stability boundary and the postfault system trajectory is presented.
- It is seen that the stability boundary as seen when projected in the angle subspace alone can be different from that of the boundary seen in the angle and speed space.
- It is observed that the postfault system trajectory leaves at different edges of the boundary depending on the fault clearing time.

6.2 Suggestions for Future Work

The following suggestions are made for further research work:

1. Analytic sensitivity analysis of the shape of the boundary with system stress.
2. The homological operator, La is sparse. For a large system, the sparsity of La can be used for efficient computation of $h2_r$ coefficients.
3. Consideration of 3^{rd} order terms in Taylor's series and consequently 3^{rd} order normal form transformation can be used to extend the stability boundary further away from the UEP.
4. For practical application for a larger system, efficient computer coding needs to be exploited.
5. It has been observed that at increased stress the SEP and the UEP tend to come close together and possibly coalesce. This phenomenon needs further investigation.

BIBLIOGRAPHY

[1] D. K. Arrowsmith and C. M. Place, *An Introduction to Dynamical Systems.* Cambridge University Press, Cambridge, 1990.

[2] V. I. Arnold, *Geometrical Methods in the Theory of Ordinary Differential Equations.* Springer-Verlag, New York, 1983.

[3] C.-M. Lin, V. Vittal, W. Kliemann, and A. A. Fouad, "Investigation of modal interaction and its effects on control performance in stressed power systems using normal forms of vector fields," in *IEEE PES Summer Meeting*, 95 SM 522-3 PWRS 1995.

[4] M. A. Pai, *Energy Function Analysis for Power System Stability.* Kluwer Academic Publishers, Boston, 1989.

[5] A. A. Fouad and V. Vittal, *Power System Transient Stability Analysis Using Transient Energy Method.* Prentice-Hall, Inc., Englewood Cliffs, NJ, 1992.

[6] H. D. Chiang, F. F. Wu, and P. P. Varaiya, "Foundations of the potential energy boundary surface method for power system transient stability analysis," *IEEE Transactions on Circuits and Systems*, vol. 35, pp. 712–728, June 1988.

[7] J. Zaborzsky, G. Huang, B. Zheng, and T. C. Leung, "On the phase-portrait of a class of large nonlinear dynamic systems such as the power system," *IEEE Transactions on Automatic Control*, vol. 33, pp. 4–15, January 1988.

[8] H. D. Chiang, F. F. Wu, and P. P. Varaiya, "Foundations of the direct methods for power system transient stability analysis," *IEEE Transactions on Circuits and Systems*, vol. CAS-34, pp. 160–172, February 1987.

[9] H. Yee, "Region of transient stability in state space for synchronous generator," *IEE Proceedings*, vol. 122, no. 7, pp. 739–744, 1975.

[10] H. Yee and B. D. Spalding, "Transient stability analysis of multimachine power systems by the method of hyperplanes," *IEEE Transactions on Power Apparatus and Systems*, vol. PAS-96, pp. 276–284, January/February 1977.

[11] F. M. A. Salam, A. Arapostathis, and P. P. Varaiya, "Analytic expressions for the unstable manifold at equilibrium points in dynamical systems of differential equations," in *22nd conference on decision and control*, pp. 1389–1392, 1983.

[12] S. Ushiki, "Analytic expressions of unstable manifolds," *Proc. Japan Acad. 56. ser. A*, pp. 239–243, 1980.

[13] P. A. Cook and A. M. Eskicioglu, "Transient stability analysis of electric power systems by the method of tangent hypersurfaces," *IEE Proceedings, Pt. C*, vol. 130, pp. 183–193, July 1983.

[14] M. Djukanovic, D. J. Sobajic, and Y.-H. Pao, "Neural-net based tangent hypersurfaces for transient security assessment of electric power systems," *Interna-*

tional Journal of Electric Power & Energy System, vol. 16, no. 6, pp. 399–408, 1994.

[15] A. H. Nayfeh, *Method of Normal Forms.* John Wiley & Sons, Inc., New York, 1993.

[16] S.-N. Chow, C. Li, and D. Wang, *Normal Forms and Bifurcation of Planer Vector Fields.* Cambridge University Press, Cambridge, 1994.

[17] S. Wiggins, *Introduction to Applied Nonlinear Dynamical Systems and Chaos.* Springer-Verlag, New York, 1990.

[18] A. A. Fouad et al, *Analysis of Stressed Interconnected Power Networks.* Electric Power Research Institute Report TR-103704, March 1994.

[19] S. K. Starrett, *Application of normal forms of vector fields to stressed power systems.* PhD thesis, Iowa State University, 1994.

[20] C.-M. Lin, *Analysis of nonlinear modal interaction and its effect on control performance in stressed power systems using normal forms method.* PhD thesis, Iowa State University, 1995.

[21] Y. Ni, V. Vittal, W. H. Kliemann, and A. A. Fouad, "Application of the normal form of vector fields to ac/dc power systems," in *27th North American Power Symposium*, (Montana), pp. 6–12, October 1995.

[22] M. W. Hirsch and S. Smale, *Differential Equations, Dynamical Systems, and Linear Algebra.* Academic Press, New York, 1974.

[23] J. Guckenheimer and P. Holmes, *Nonlinear Oscillation, Dynamical System and Bifurcation of Vector Fields.* Springer-Verlag, New York, 1983.

[24] P. M. Anderson and A. A. Fouad, *Power System Control and Stability.* IEEE Press, 1994.

[25] S. Saha, V. Vittal, W. Kliemann, and A. A. Fouad, "Local approximation of stability boundary of a power system using the real normal form of vector fields," in *Proc. IEEE International Symposium of Circuits & Systems*, (Seattle), pp. 2330–2333, 1995.

[26] C. Elphick, E. Tirapegui, M. E. Brachet, P. Coullet, and G. Iooss, "A simple global characterization for normal forms of singular vector fields," *Physica*, vol. 29D, pp. 95–127, 1987.

[27] L. O. Chua and H. Kokubu, "Normal forms for nonlinear vector fields – part I: Theory and algorithm," *IEEE Transactions on Circuits and Systems*, vol. 35, pp. 863–880, July 1988.

[28] L. O. Chua and H. Kokubu, "Normal forms for nonlinear vector fields – part II: Applications," *IEEE Transactions on Circuits and Systems*, vol. 36, pp. 51–70, January 1989.

[29] I. J. Perez-Arriaga, G. C. verghese, and F. C. Schweppe, "Selective modal analysis with application to electric power systems," *IEEE Transactions on Power Apparatus and Systems*, vol. PAS-101, pp. 3117–3125, September 1982.

[30] C. J. Tavora and O. J. M. Smith, "Characterization of equilibrium and stability in power systems," *IEEE Transactions on Power Apparatus and Systems*, vol. PAS-91, pp. 1127–1130, May/June 1972.

[31] Electric Power Research Institute, "Transient energy function program user's manual, TEF version 3.0," Palo Alto, California, September 1991.

[32] Electric Power Research Institute, "Transient energy function program user's manual, TEF version 1.2," Palo Alto, California, December 1987.

[33] S. Saha, W. Kliemann, V. Vittal, and A. A. Fouad, "Effect of stress on the boundary of stability of a power system," in *27th North American Power Symposium*, (Montana), pp. 257–262, October 1995.

[34] V. Vittal, S. Rajagopal, P. Movall, and A. A. Fouad, "Analysis of potential energy surfaces of multimachine power systems using computer graphics," *IEEE Transactions on Education*, vol. E-29, pp. 181–185, November 1986.

[35] B. Berggren and G. Andersson, "On the nature of unstable equilibrium points in power systems," *IEEE Transactions on Power Systems*, pp. 738–744, May 1993.

[36] R. W. Brankin, I. Gladwell, and L. F. Shampine, "RKSUITE." Release 1.0, November 1991.

[37] Electric Power Research Institute, "Extended transient-midterm stability program (ETMSP): Version 3.1," Palo Alto, California, May 1994.

[38] H. D. Chiang, J. Tong, and K. N. Miu, "Predicting unstable modes in power systems: Theory and computations," *IEEE Transactions on Power Systems*, vol. 8, pp. 1429–1435, November 1993.

ACKNOWLEDGMENTS

It is my pleasure to express gratitude to my major professor Dr. Aziz A. Fouad, Distinguished Professor, Department of Electrical and Computer Engineering, Iowa State University, Ames, under whose able guidance the work is conducted. His keen interest in the problem and encouragement at every stage of the work were always a great source of inspiration to me. I am also thankful to Dr. Fouad for providing financial support during my Ph.D program.

My sincere thanks to Dr. V. Vittal and Dr. W. H. Kliemann for generously providing time and assistance in the completion of this work. I also thank Dr. J. D. McCalley and Dr. M. H. Khammash for serving as committee members and Dr. V. Ajjarapu for serving as a substitute for Dr. M Khammash in my final examination.

The author acknowledges the financial supports of the Electric Power Research Institute and the U. S. National Science Foundation for this research work.

It has been a great pleasure to be a part of power graduate students group at Iowa State University which made my stay enjoyable. I thank them all.

I am grateful for the support and encouragement of my family members during my entire student life. I thank my wife, Anushree for her understanding, support and encouragement in the later part of this work.

APPENDIX A. JACOBIAN AND HESSIAN MATRICES

A.1 Jacobian Matrix

The system is given by the following equations:

$$\begin{aligned}
\dot{\delta_{in}} &= \omega_{in} \quad for \;\; i = 1, n-1 \\
\dot{\omega_{in}} &= \frac{1}{M_i}\left(P_{mi} - E_i^2 G_{ii}\right) - \frac{1}{Mn}\left(P_{mn} - E_n^2 G_{nn}\right) \\
&\quad -\frac{1}{M_i}\left[E_i E_n Y_{in}\cos\left(\delta_{in} - \theta_{in}\right) + \sum_{j=1, j\neq i}^{n-1} E_i E_j Y_{ij}\cos\left(\delta_{in} - \delta_{jn} - \theta_{ij}\right)\right] \\
&\quad +\frac{1}{Mn}\left[\sum_{j}^{n-1} E_j E_n Y_{jn}\cos\left(\delta_{jn} + \theta_{jn}\right)\right] - c\omega_{in} \qquad i = 1, ..., n-1 \qquad \text{(A.1)}
\end{aligned}$$

The above $2(n-1)$ equations can be written as vectors:

$$\begin{aligned}
\dot{\underline{\delta}} &= \underline{\omega} \\
\dot{\underline{\omega}} &= \underline{f}(\underline{\delta}) - c\,\underline{\omega} \qquad \text{(A.2)}
\end{aligned}$$

where $\underline{\delta}$ and $\underline{\omega}$ are $(n-1)$ vectors of the relative angles δ_{in} and relative speeds ω_{in}.

The Jacobian matrix of the above system has the following form:

$$\begin{bmatrix} \underline{0} & \underline{I} \\ \underline{J} & -c\underline{I} \end{bmatrix}$$

where $\underline{0}$ and $\underline{I}$ are the $(n-1) \times (n-1)$ zero and unity matrices respectively and

$$\underline{J} = \frac{\partial}{\partial \underline{\delta}} \underline{f}(\underline{\delta}) \tag{A.3}$$

The diagonal elements of J are:

$$\begin{aligned} J_{ii} &= \frac{1}{M_i}\left[A_{in}\sin(\delta_{in}-\theta_{in}) + \sum_{j=1,j\neq i}^{n-1} A_{ij}\sin(\delta_{in}-\delta_{jn}-\theta_{ij})\right] \\ &\quad -\frac{1}{M_n}A_{in}\sin(\delta_{in}+\theta_{in}) \end{aligned} \tag{A.4}$$

and the off-diagonal elements are:

$$J_{ij} = -\frac{1}{M_i}A_{ij}\sin(\delta_{in}-\delta_{jn}-\theta_{ij}) - \frac{1}{M_n}A_{jn}\sin(\delta_{jn}+\theta_{jn}) \tag{A.5}$$

where, $A_{ij} = E_i E_j Y_{ij}$.

A.2 Hessian Matrices

The Hessian matrices of $f_i(\underline{\delta})$ is denoted by H^i, and is defined as

$$H^i = \left[\frac{\partial^2 f_i(\underline{\delta})}{\partial\delta_{jn}\partial\delta_{kn}}\right] \quad j = 1,..,n-1,\ k = 1,..,n-1 \ \ \forall i \tag{A.6}$$

$$\begin{aligned} \frac{\partial^2 f_i(\underline{\delta})}{\partial\delta_{in}^2} &= \frac{1}{M_i}\left[A_{in}\cos(\delta_{in}-\theta_{in}) + \sum_{j=1,j\neq i}^{n-1} A_{ij}\cos(\delta_{in}-\delta_{jn}-\theta_{ij})\right] \\ &\quad -\frac{1}{M_n}A_{in}\cos(\delta_{in}+\theta_{in}) \ \ i = 1,..,n-1 \end{aligned} \tag{A.7}$$

For $i \neq k$

$$\frac{\partial^2 f_i(\underline{\delta})}{\partial\delta_{in}\delta_{kn}} = -\frac{1}{M_i}A_{ik}\cos(\delta_{in}-\delta_{kn}-\theta_{ik}) \ \ i = 1,..,n-1 \tag{A.8}$$

For $i \neq k$

$$\frac{\partial^2 f_i(\underline{\delta})}{\partial \delta_{kn}^2} = \frac{A_{ik}}{M_i}\cos(\delta_{in} - \delta_{kn} - \theta_{ik}) - \frac{A_{kn}}{M_n}\cos(\delta_{kn} + \theta_{kn})\ i = 1, .., n-1 \quad \text{(A.9)}$$

And for $i \neq j,\ j \neq k,\ k \neq i$

$$\frac{\partial^2 f_i(\underline{\delta})}{\partial \delta_{jn} \delta_{kn}} = 0 \quad \text{(A.10)}$$

APPENDIX B. DATA FOR 11 GENERATOR TEST SYSTEM

B.1 Dynamic Data for 11 Generator Test System

The inertia constants, H and direct axis transient reactance on 100 MVA base of the 11 generator test system are given in Table B.1. M and H are related as, $M = \frac{2H}{377}$.

Table B.1: H and $x_{d'}$

Bus #	H(sec)	$x_{d'}$
54	241.000	0.00393
458	74.400	0.01280
733	73.850	0.01220
784	28.140	0.06233
968	73.850	0.01220
975	57.520	0.04803
991	115.040	0.02402
1001	105.792	0.01797
2001	109.960	0.00848
2018	207.230	0.00451
2192	9344.170	0.00010

B.2 Load Flow Data for 11 Generator Test System

Tables B.2 and B.3 provide bus and branch data for 11 generator test system.

Table B.2: 11 generator bus data

Serial #	Bus #	Vol Mag p.u.	Vol Angle Deg	P_{load} MW	Q_{load} MVAR	P_{gen} MW	Q_{gen} MVAR
1	3	1.0740	19.06	-4.85	-90.83	0.00	0.00
2	5	1.0829	19.50	250.39	480.10	0.00	0.00
3	7	1.0929	19.52	228.02	77.17	0.00	0.00
4	8	1.0693	21.76	6.35	221.21	0.00	0.00
5	24	1.0826	12.97	341.12	244.28	0.00	0.00
6	30	1.1331	10.69	432.69	111.05	0.00	0.00
7	33	1.1384	15.38	497.84	-88.98	0.00	0.00
8	37	1.1505	20.99	235.69	-12.89	0.00	0.00
9	39	1.1520	23.01	43.70	-6.79	0.00	0.00
10	40	1.1519	22.99	43.80	-6.88	0.00	0.00
11	43	1.1330	22.56	45.88	3.64	0.00	0.00
12	44	1.1344	22.42	45.87	3.64	0.00	0.00
13	47	1.1231	24.01	945.23	-374.91	0.00	0.00
14	48	1.1391	31.59	71.72	186.88	0.00	0.00
15	54	1.0909	30.20	4114.20	1365.20	6357.47	1814.30
16	80	1.0532	17.66	920.78	-75.58	0.00	0.00
17	140	1.1491	21.19	18.08	10.25	0.00	0.00
18	141	1.1491	21.19	17.98	10.22	0.00	0.00
19	142	1.1469	22.08	19.72	13.77	0.00	0.00
20	143	1.1469	22.08	19.70	13.80	0.00	0.00
21	144	1.1478	23.19	40.54	30.29	0.00	0.00
22	145	1.1639	31.60	30.77	-3.79	0.00	0.00
23	146	1.1639	31.60	30.86	-3.81	0.00	0.00
24	148	1.1456	20.17	17.18	9.37	0.00	0.00
25	149	1.1456	720.17	17.18	9.37	0.00	0.00
26	150	1.1461	719.51	233.50	31.41	0.00	0.00
27	226	1.1813	37.34	0.00	0.00	0.00	0.00
28	288	1.1733	34.15	52.18	-3.29	0.00	0.00

Table B.2 (Continued)

29	297	1.1183	16.37	2049.10	-667.91	0.00	0.00
30	458	1.0667	24.63	644.56	285.91	1669.37	106.74
31	617	1.1606	30.75	38.70	2.76	0.00	0.00
32	618	1.1608	30.78	38.66	2.74	0.00	0.00
33	644	1.0749	13.73	115.54	-537.09	0.00	0.00
34	733	1.0000	39.04	31.64	20.00	1999.20	161.66
35	784	1.0000	15.64	887.73	926.25	500.00	329.43
36	963	1.0521	19.58	0.00	0.00	0.00	0.00
37	967	1.0766	32.18	-8.41	-156.82	0.00	0.00
38	968	1.0000	37.42	31.64	20.00	1999.20	673.16
39	975	1.0000	37.98	28.00	29.00	100.00	21.77
40	977	1.1841	36.21	22.10	-7.04	0.00	0.00
41	989	1.0987	40.34	0.00	0.00	0.00	0.00
42	991	1.0000	40.90	57.00	59.00	200.00	123.41
43	992	1.1813	36.88	0.00	0.00	0.00	0.00
44	993	1.0495	19.45	193.17	378.30	0.00	0.00
45	994	1.0495	19.45	190.93	374.18	0.00	0.00
46	996	1.0536	18.80	-7.12	-107.08	0.00	0.00
47	1000	1.0989	40.47	0.00	0.00	0.00	0.00
48	1001	1.0000	44.47	360.00	360.00	1300.00	459.43
49	1060	1.1785	37.16	2.73	2.12	0.00	0.00
50	1106	0.9883	14.27	184.83	199.34	0.00	0.00
51	2001	0.9664	4.23	2632.00	498.53	2827.60	141.27
52	2018	1.0895	26.35	4244.60	805.48	5329.50	1777.66
53	2192	1.0340	14.05	235100.00	62413.00	241884.73	63475.55
54	2317	1.0600	-5.54	8783.70	-517.70	0.00	0.00
55	2325	1.0695	9.38	471.40	-151.14	0.00	0.00

Table B.3: 11 generator line data

From Bus	To Bus	R, p.u	X,p.u.	B, p.u	Off-nominal tap
3	5	0.003520	0.036720	3.45154	0.0000
3	5	0.003390	0.036690	3.45813	0.0000
3	150	0.000300	0.018200	0.00000	0.9259
3	150	0.000300	0.020300	0.00000	0.9259
3	996	0.000960	0.009080	0.85556	0.0000
3	996	0.000960	0.009080	0.85556	0.0000
5	7	0.002280	0.027560	2.62024	0.0000
5	458	0.000640	0.034460	0.00000	1.0000
7	8	0.001730	0.020750	1.96472	0.0000
7	458	0.041050	0.393870	0.00000	1.0000
8	458	0.001280	0.026470	0.00000	1.0000
24	30	0.003380	0.029770	0.00000	0.0000
24	33	-0.052620	1.383430	0.00000	0.0000
24	33	0.012920	0.112030	0.18075	0.0000
24	33	0.012920	0.112050	0.18073	0.0000
24	33	0.005740	0.060520	0.00000	0.0000
24	644	0.000100	0.005460	0.00000	1.0000
30	33	0.016010	0.099370	0.15627	0.0000
30	33	0.016040	0.099390	0.15623	0.0000
30	644	-0.001620	0.077330	0.00000	1.0000
33	37	0.008120	0.078180	0.13190	0.0000
33	37	0.008120	0.078180	0.13190	0.0000
33	47	0.010010	0.098760	0.15844	0.0000
33	47	0.003290	0.046510	0.00000	0.0000
33	644	0.028260	0.461480	0.00000	1.0000
37	39	0.005010	0.034670	0.05207	0.0000
37	40	0.005010	0.034660	0.05207	0.0000
37	43	0.002400	0.031800	0.05672	0.0000
37	44	0.002400	0.031800	0.05671	0.0000
37	140	0.001410	0.008720	0.01366	0.0000
37	141	0.001410	0.008720	0.01366	0.0000
39	40	0.030620	0.809460	0.00000	0.0000
39	40	-0.035640	0.543650	0.00000	0.0000
39	617	0.014490	0.113180	0.00000	0.0000
39	618	0.000240	0.870170	0.00000	0.0000

Table B.3 (Continued)

40	617	0.000240	0.870170	0.00000	0.0000
40	618	0.015110	0.115070	0.00000	0.0000
43	44	-0.023140	0.377740	0.00000	0.0000
43	47	0.001800	0.020100	0.03459	0.0000
44	47	0.001800	0.024000	0.04222	0.0000
47	48	0.003500	0.044490	0.07339	0.0000
47	48	0.003500	0.044490	0.07339	0.0000
47	48	0.002700	0.031800	0.11433	0.0000
47	48	0.003520	0.044730	0.07386	0.0000
47	48	0.003520	0.044730	0.07386	0.0000
47	54	0.001540	0.023400	0.00000	1.0000
47	80	0.021770	0.479680	0.00000	1.0000
47	297	0.004330	0.039990	0.00000	1.0000
47	458	0.032940	0.771160	0.00000	1.0000
47	644	-0.168360	2.246910	0.00000	1.0000
47	784	0.157880	1.518370	0.00000	1.0000
47	784	0.059910	0.936860	0.00000	1.0000
47	784	0.109310	1.701790	0.00000	1.0000
47	993	0.000580	0.078940	0.00000	1.0000
47	994	0.000560	0.079840	0.00000	1.0000
47	1106	0.157990	1.520600	0.00000	1.0000
47	2018	-0.017990	0.445020	0.00000	1.0000
47	2317	-1.056490	4.386920	0.00000	1.0000
48	733	0.000600	0.025700	0.00000	1.1435
48	733	0.000600	0.026500	0.00000	1.1435
48	733	0.000600	0.026500	0.00000	1.1435
48	733	0.000600	0.026500	0.00000	1.1435
967	48	0.000300	0.018100	0.00000	0.9167
967	48	0.000300	0.016300	0.00000	0.9167
54	80	-0.000780	0.076070	0.00000	1.0000
54	297	0.005750	0.157510	0.00000	1.0000
54	458	0.005910	0.739670	0.00000	1.0000
54	644	-0.014740	0.096690	0.00000	1.0000
54	784	0.002430	0.812190	0.00000	1.0000
54	784	-0.002370	0.751970	0.00000	1.0000
54	784	0.001210	0.447110	0.00000	1.0000
54	993	-0.025040	0.528020	0.00000	1.0000

Table B.3 (Continued)

54	994	-0.025450	0.534040	0.00000	1.0000
54	1106	-0.002430	0.753070	0.00000	1.0000
54	2001	-0.096710	0.419510	0.00000	1.0000
54	2018	-0.002990	0.025740	0.00000	1.0000
54	2192	-0.188400	0.877980	0.00000	1.0000
54	2317	-0.115110	0.331850	0.00000	1.0000
80	297	-0.000800	0.040080	0.00000	1.0000
80	458	-0.031240	0.478100	0.00000	1.0000
80	784	-0.004440	0.106330	0.00000	1.0000
80	784	-0.004600	0.094580	0.00000	1.0000
80	784	-0.002460	0.058540	0.00000	1.0000
80	993	-0.031210	0.659410	0.00000	1.0000
80	994	-0.031730	0.666930	0.00000	1.0000
80	996	0.000530	0.005840	0.60400	0.0000
80	996	0.000530	0.005840	0.60400	0.0000
80	1106	-0.004610	0.094720	0.00000	1.0000
80	2018	-0.056810	0.548510	0.00000	1.0000
140	141	-0.062300	0.927530	0.00000	0.0000
140	142	0.004780	0.029280	0.04586	0.0000
141	143	0.004780	0.029280	0.04586	0.0000
142	143	-0.005500	0.383150	0.00000	0.0000
142	144	0.004670	0.028850	0.04519	0.0000
143	144	0.004670	0.028850	0.04519	0.0000
144	145	0.008950	0.077910	0.12311	0.0000
144	146	0.008950	0.077910	0.12311	0.0000
144	148	0.007590	0.048320	0.07128	0.0000
144	149	0.007590	0.048320	0.07128	0.0000
145	146	-0.005010	0.208210	0.00000	0.0000
145	226	0.005640	0.050370	0.07944	0.0000
145	288	0.085750	0.568540	0.00000	0.0000
146	226	0.005640	0.050370	0.07944	0.0000
146	288	0.085500	0.567040	0.00000	0.0000
148	149	-0.002830	0.382420	0.00000	0.0000
148	150	0.001880	0.011980	0.01769	0.0000
149	150	0.001880	0.011980	0.01769	0.0000
150	288	0.066340	0.555860	0.00000	0.0000
150	297	0.028270	0.247970	0.00000	0.0000

Table B.3 (Continued)

150	458	0.014190	0.155890	0.00000	1.0000
226	288	0.009950	0.063350	0.11046	0.0000
226	617	0.007650	0.071990	0.10050	0.0000
226	618	0.007650	0.072000	0.10050	0.0000
226	975	0.000240	0.015630	0.00000	1.1801
226	977	0.009950	0.070690	0.11169	0.0000
989	226	0.000300	0.017900	0.00000	0.9259
989	226	0.000300	0.017900	0.00000	0.9259
989	226	0.000300	0.017900	0.00000	0.9259
226	992	0.000200	0.021800	0.00000	0.0000
226	992	0.000200	0.022000	0.00000	0.0000
226	992	0.000180	0.022150	0.00000	0.0000
226	1060	0.000000	0.158000	0.00000	0.0000
288	977	-0.005660	0.325930	0.00000	0.0000
297	458	-0.000120	0.050630	0.00000	1.0000
297	784	0.004860	0.127190	0.00000	1.0000
297	784	-0.000120	0.078270	0.00000	1.0000
297	784	-0.000180	0.142180	0.00000	1.0000
297	993	0.000830	0.055210	0.00000	1.0000
297	994	0.000820	0.055840	0.00000	1.0000
996	297	0.000300	0.019200	0.00000	0.9167
996	297	0.000300	0.018800	0.00000	0.9167
996	297	0.000300	0.019200	0.00000	0.9167
297	1106	0.004860	0.127370	0.00000	1.0000
297	2018	-0.266020	2.781220	0.00000	1.0000
458	784	-0.026010	1.432810	0.00000	1.0000
458	784	-0.072710	2.173670	0.00000	1.0000
458	784	-0.014540	0.788760	0.00000	1.0000
458	993	-0.053110	1.057950	0.00000	1.0000
458	994	-0.053970	1.070020	0.00000	1.0000
458	1106	-0.072990	2.176840	0.00000	1.0000
617	618	-0.034810	0.934120	0.00000	0.0000
617	618	0.012240	0.597670	0.00000	0.0000
644	2001	-0.414030	1.712200	0.00000	1.0000
644	2018	-0.050240	0.272610	0.00000	1.0000
644	2192	-0.000560	0.005790	0.00000	1.0000
644	2317	-0.057280	0.242950	0.00000	1.0000

Table B.3 (Continued)

784	993	0.022650	2.095820	0.00000	1.0000
784	993	-0.037310	1.288360	0.00000	1.0000
993	784	-0.067110	2.340360	0.00000	1.0000
784	994	0.022410	2.119770	0.00000	1.0000
784	994	-0.038040	1.303070	0.00000	1.0000
994	784	-0.068440	2.367080	0.00000	1.0000
784	1106	0.000790	0.178760	0.00000	0.0000
784	1106	-0.079710	0.777450	0.00000	1.0000
784	1106	-0.144390	1.412310	0.00000	1.0000
963	967	0.001290	0.013850	1.46527	0.0000
963	993	0.000160	0.001680	0.17525	0.0000
963	994	0.000160	0.001680	0.17529	0.0000
963	996	0.000190	0.002030	0.87993	0.0000
963	996	0.000190	0.002030	0.87993	0.0000
967	968	0.000100	0.018100	0.00000	1.1053
967	968	0.000100	0.018100	0.00000	1.1053
967	968	0.000100	0.018100	0.00000	1.1053
967	968	0.000100	0.018100	0.00000	1.1053
989	991	0.000240	0.013740	0.00000	1.1037
989	991	0.000240	0.013680	0.00000	1.1037
989	992	-0.008600	0.165790	0.00000	0.9259
989	992	-0.008700	0.167400	0.00000	0.9259
989	992	-0.008990	0.171790	0.00000	0.9259
989	1000	0.000030	0.000580	0.06315	0.0000
989	1000	0.000030	0.000580	0.06315	0.0000
993	994	-0.009390	0.109190	0.00000	0.0000
993	1106	0.022530	2.098890	0.00000	1.0000
994	1106	0.022280	2.122870	0.00000	1.0000
1000	1001	0.000180	0.014770	0.00000	1.1053
1000	1001	0.000180	0.014770	0.00000	1.1053
2001	2018	-0.014240	0.070820	0.00000	1.0000
2001	2192	-0.160380	0.650650	0.00000	1.0000
2001	2317	-0.005240	0.021160	0.00000	1.0000
2018	2192	-0.654290	2.050080	0.00000	1.0000
2018	2317	-0.020600	0.064670	0.00000	1.0000
2192	2317	-0.001120	0.005620	0.00000	1.0000
2192	2325	-0.002450	0.019870	0.00000	1.0000